arXiv:2510.16333v2 [cs.CV] 13 Apr 2026

RL makes MLLMs see better than SFT

Junha Song[1,2], **Sangdoo Yun**[2], **Dongyoon Han**[2], **Jaegul Choo**[1], **Byeongho Heo**[2†]

[1]KAIST, [2]NAVER AI Lab
[†]Corresponding author

A dominant assumption in Multimodal Language Model (MLLM) research is that its performance is largely inherited from the LLM backbone, given its immense parameter scale and remarkable capabilities. This has created a void in the understanding of the vision encoder, which determines '*how MLLMs perceive images*'. The recent shift in MLLM training paradigms, from Supervised Finetuning (SFT) to Reinforcement Learning (RL), magnifies this oversight—namely, the significant lack of analysis on how such training reshapes the vision encoder as well as the MLLM. To address this, we first investigate the impact of training strategies on MLLMs, where RL shows a clear advantage over SFT in strongly vision-related VQA benchmarks. Motivated by this, we conduct a critical yet under-explored analysis of the vision encoder of MLLMs through diverse and in-depth experiments, ranging from ImageNet classification and segmentation to gradient visualization. Our results demonstrate that MLLM's post-training strategy (*i.e.*, SFT or RL) not only leads to distinct outcomes on MLLM downstream tasks, but also fundamentally reshapes MLLM's underlying visual representations. Specifically, our main finding is that **RL produces stronger and more localized visual representations compared to SFT, boosting the ability of the vision encoder for MLLM.** We then reframe our findings into a simple recipe for building strong vision encoders for MLLMs, Preference-Instructed Vision OpTimization (PIVOT). When integrated into MLLMs, a PIVOT-trained vision encoder outperforms even larger and more heavily-trained counterparts, despite requiring less than 1% of the computational cost of standard vision pretraining. This result opens an effective and efficient path for advancing the vision backbones of MLLMs.

Date: April 14, 2026
Project page: https://june-page.github.io/pivot/

1 Introduction

Human knowledge is acquired through multiple sensory experiences, with vision playing a dominant role in understanding the environment and accumulating knowledge, beyond finding food and avoiding predators (Piaget et al., 1952; Tong et al., 2024a). Inspired by this principle, recent advances in Large Language Models (LLMs) (Dubey et al., 2024; Yang et al., 2025b; Brown et al., 2020) naturally extend toward Multimodal LLMs (MLLMs) (Achiam et al., 2023; Team et al., 2023, 2024a). Especially, large vision language models[1] have been recently and preferentially investigated as a pathway to foster visual intelligence in LLMs (Liu et al., 2023a; Li et al., 2025a; Chen et al., 2024).

The combination of independently pretrained LLMs and vision models enabled MLLMs to reach strong initial capabilities (Mokady et al., 2021; Li et al., 2023a). Further advances have been driven by larger and stronger architectures, along with higher-quality datasets, as shown in LLaVA (Liu et al., 2024a; Li et al., 2025a), QwenVL (Bai et al., 2023b), and DINO-MLLM (Fan et al., 2025). Building on this, current research now seeks improvements via reinforcement learning (RL), moving beyond the standard supervised finetuning (SFT), paralleling the shift that RL brought to LLMs (Christiano et al., 2017; Ouyang et al.,

[1]Following recent works (Tong et al., 2024a,b; Fan et al., 2025), we refer to LLMs with visual capabilities as MLLMs.

2022). For instance, several studies demonstrate that incorporating human preference data via RL enhances MLLM performance (Sun et al., 2024; Wang et al., 2024b) and mitigates hallucination (Yang et al., 2025c; Yu et al., 2024; Fu et al., 2025b). Other research has expanded the scope of RL to include contrastive image pairs (Wang et al., 2024a; Fu et al., 2025a).

Despite the efficacy of RL in the **MLLM**, a comprehensive understanding of its effects compared to SFT—and critically, its influence on the **vision encoder**—remains largely absent from the literature. Specifically, the field lacks a systematic comparison within MLLMs between SFT for instruction-following and RL for preference alignment, including an analysis of model scaling in common benchmarks. The lack of understanding is especially notable for another under-investigated dimension: the vision encoder. Indeed, research has progressed little beyond the preliminary finding that fine-tuning the vision encoder (Tong et al., 2024a; Li et al., 2024b) yields better outcomes than keeping it frozen (Liu et al., 2023a; Li et al., 2023a; Driess et al., 2023; Karamcheti et al., 2024). Such oversight can be attributed to an implicit, LLM-centric assumption about the source of MLLM capabilities, leaving a significant void in our understanding of how SFT and RL differ in reshaping visual representations.

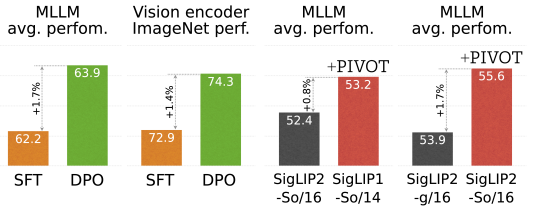


Figure 1 TL;DR. We study how SFT and RL (*e.g.*, DPO) affect not only MLLMs but also their vision encoders, and formulate a simple recipe, PIVOT, for evolving vision models for use in MLLM.

We present a timely exploration of both the MLLM and its vision encoder under different training strategies. We focus our RL analysis on Direct Preference Optimization (DPO) for simplicity, which is a common recipe for recent MLLMs (Yu et al., 2024; Yang et al., 2025c; Fu et al., 2025a). We begin with a fundamental analysis in Section 3, comparing the effects of SFT and RL on MLLMs across broad vision-language (VL) benchmarks. Our analysis reveals that RL yields significant gains on vision-centric tasks, a finding that motivates a deeper investigation into the vision encoder itself. Subsequently, in Section 4, we conduct a unique and critical analysis of the vision encoder, providing key insights for the visual encoder development. Our results reveal that MLLM post-training rewrites the visual representations, with RL driving stronger representation than SFT. The finding is supported by gradient visualizations that trace how optimization signals propagate to the vision encoder.

The foregoing analysis establishes that RL reshapes visual representations, motivating a critical question we explore in Section 6: *Can RL-trained models surpass SOTA vision models for MLLM?*. To this end, we re-formalize RL training as an auxiliary training process for vision encoder, termed Preference-Instructed Vision OpTimization (PIVOT), and evaluate its efficacy on diverse encoders, including CLIP (Radford et al., 2021), DINO (Oquab et al., 2024), and MAE (He et al., 2022). The results reveal a remarkable impact of PIVOT when the enhanced encoders are used within MLLMs; a vision model trained with PIVOT not only outperforms its original counterpart but also surpasses a substantially larger model (*e.g.*, SigLIP2-So/16 + PIVOT > SigLIP2-g/16) and even a subsequent-generation encoder (*e.g.*, SigLIP1-So/14[2] + PIVOT > SigLIP2-So/16). Notably, this enhancement is achieved with just 18 hours of training on 8 H100 GPUs using a Qwen2.5-1.5B LLM-head. This amounts to fewer than **1%** of GPUs of standard vision pre-training, with SigLIP2 trained on up to 2K TPUv5e chips. Taken together, the evidence indicates that even state-of-the-art encoders have substantial room for MLLM evolution, and PIVOT is a promising direction for future exploration.

2 MLLMs on RL: Where do we stand?

The initial paradigm for training LLMs involves auto-regressive pre-training followed by SFT to promote instruction-following capabilities (Radford et al., 2018; Dai et al., 2019; Yang et al., 2019; Brown et al., 2020). A subsequent breakthrough occurs with Reinforcement Learning from Human Feedback (RLHF), which demonstrates that utilizing RL to align LLM outputs with human preferences enables chat-oriented LLMs (Christiano et al., 2017; Ouyang et al., 2022; Touvron et al., 2023b). The use of RL has become a

[2]We use SigLIP1-So/14, as the weights for SigLIP1-So/16 are not publicly available.

cornerstone of modern LLM development, with advanced methods like DPO (Rafailov et al., 2023) and GRPO (Shao et al., 2024) being widely implemented in recent models such as LLaMA-3 (Dubey et al., 2024) and Qwen-2.5 (Yang et al., 2025a).

MLLMs have adopted the LLM training advances to leverage prior experiences. Early MLLMs such as LLaVA-Next (Li et al., 2024b) and Cambrian (Tong et al., 2024a) combine a pre-trained LLM with a pre-trained vision model, then align the LLM to vision representation through **SFT** on vision-language data like captioning and visual question answering. Recent works, as summarized in Table A, demonstrated that applying **RL** as an auxiliary process can further boost MLLM's downstream performance (Yu et al., 2025; Wang et al., 2024b; Sun et al., 2024). Other studies have proposed advanced DPO variants for multimodal contexts, for instance by incorporating visual preference data (Fu et al., 2025a; Wang et al., 2024a) or modifying the objective to mitigate hallucinations (Yu et al., 2024; Yang et al., 2025c). Further studies highlight RL's advantages over SFT in adapting an MLLM's knowledge to specialized environments, such as map navigation (Chu et al., 2025) and robot action planning (Li et al., 2025b).

These studies reveal a clear trend in the application of RLHF to MLLMs. They rely on RL using either PPO (Sun et al., 2024) or DPO, with the predominant choice becoming DPO, as shown in Table A. Following this trend, our main paper adopts DPO as the primary RL representative for a controlled comparison with SFT.

3 How do SFT and RL affect MLLMs?

Despite the advances of RL described in Section 2, existing studies lack a comprehensive analysis, offering limited insight and intuition into the following questions: *How do SFT and DPO affect MLLM on diverse VQA tasks?*, *Is DPO actually superior to SFT?*, and *does this trend hold with model scaling?* To address them, we establish a controlled training setup and conduct a deep investigation.

3.1 Experimental setup & prerequisite

Model scaling. The standard MLLM architecture, which integrates an LLM with a vision encoder via a multimodal projector, has proven effective in achieving superior performance on VL tasks (Lei et al., 2025; Shukor et al., 2025). Our model is implemented using the popular open-source MLLM repository, LLaVA-OneVision (Li et al., 2025a). Following their setup, we conduct a study across various cases by adopting four scales of the Qwen2.5 LLM (0.5B, 1.5B, 3B, 7B) (Yang et al., 2025a) and four SigLIP2 384px sizes (B/16, L/16, So/16, g/16) (Tschannen et al., 2025), with a 2-layer MLP serving as the projector.

Training procedure. Our MLLM development process consists of two stages: *Stage 1* pre-training and *Stage 2* post-training. In *Stage 1*, we first align the visual and language embedding spaces by conducting multimodal projector-only training. Then, a base MLLM is established by training all model parameters on diverse VL datasets, including Visual Question Answering (VQA), vision-grounded dialogue, and image captioning (Li et al., 2025a). *Stage 2* indicates post-training, which involves a full-parameter update of the base model according to SFT or DPO, detailed below. Further details, including hyperparameters, are included in Section E.1 and the source code[3].

Post-training strategies. Our analysis compares two post-training approaches: SFT and DPO. Prior works like MPO (Wang et al., 2024b) typically focus on comparing a pre-trained model (*Stage 1*) against the same model further trained with DPO, which does not provide a fair evaluation of DPO versus SFT. On the other hand, we conduct a controlled comparison in *Stage 2*, using the *same* number of 'image-query-response' pairs across the two algorithms. Specifically, we define the post-training dataset as $X_{\text{PT}} = \{x_0, x_1, \ldots, x_T\}$, with each element $x_i = \{I_i, q_i, y_i^c, y_i^r\}$ representing an image I_i, a query q_i, and the corresponding chosen and rejected responses y_i^c and y_i^r. The optimization objectives using this dataset are defined as follows:

$$L_{\text{SFT}} = -\mathbb{E}_{i\sim X_{\text{PT}}} \log \pi_\theta(y_i^c \mid I_i, q_i); \; L_{\text{DPO}} = -\mathbb{E}_{i\sim X_{\text{PT}}} \log \sigma\left(\beta\left(\log \frac{\pi_\theta(y_i^c|I_i,q_i)}{\pi_{\text{ref}}(y_i^c|I_i,q_i)} - \log \frac{\pi_\theta(y_i^r|I_i,q_i)}{\pi_{\text{ref}}(y_i^r|I_i,q_i)}\right)\right), \quad (1)$$

[3] https://github.com/junha1125/PIVOT

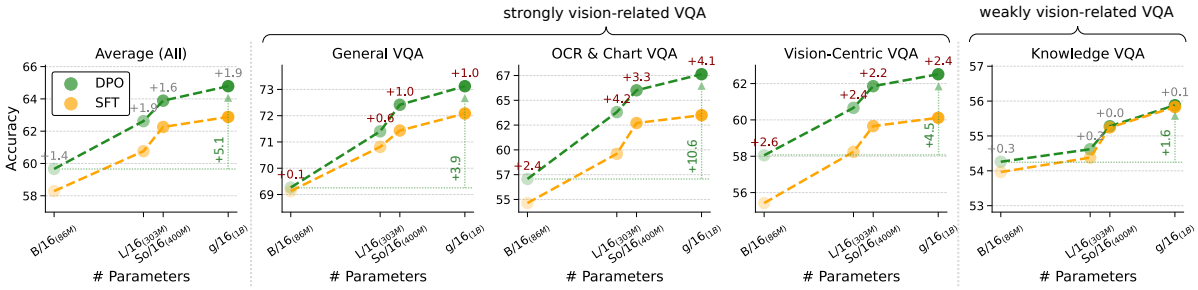


Figure 2 Scaling the vision encoder in MLLMs. We analyze the impact of the vision encoder sizes, ranging from 86M (B/16) to 1B (g/16) parameters, in Qwen2.5-3B combined with SigLIP2 on vision–language benchmarks. Interestingly, DPO yields particularly strong gains over SFT in vision-intensive VQA.

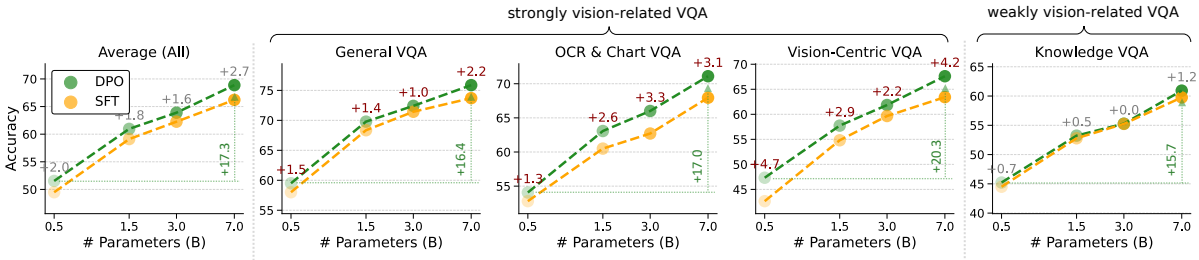


Figure 3 Scaling the language model in MLLMs. Using SigLIP2-So/16 as the vision encoder, we vary the language model size (Qwen2.5) and evaluate performance. Consistent with Figure 2, DPO substantially outperforms SFT on vision-related tasks, while they show comparable results in Knowledge VQA.

where π_θ represents the MLLM; π_{ref} is the reference model; and β is the temperature controlling the strength of preference alignment. In short, we compare SFT (*Stage 2*) with DPO (*Stage 2*) with the same number of training samples. A more detailed description is given in Section D.1.

Data & Evaluation. To ensure reproducibility, we utilize publicly available datasets provided in the LLaVA-OneVision and MPO repositories. To be more specific, in *Stage 1*, we apply projector-only pre-training on the LAION/CC/SBU-558K dataset (Liu et al., 2024a) and perform end-to-end pre-training on the LLaVA-OneVision-3.2M dataset (Li et al., 2025a). As the post-training dataset X_{pt} in *Stage 2*, we utilize the MPO (Wang et al., 2024b) data and randomly sample 20K instances, a scale comparable to recent DPO studies for MLLMs (Yu et al., 2024; Yang et al., 2025c). It is worth noting that this two-stage strategy and the proportion of training data closely resemble the training paradigm of LLMs such as InstructGPT (Ouyang et al., 2022), where RLHF is applied after instruction-following pre-training. For evaluation, we adapt the benchmark suite introduced in Cambrian, which covers 16 tasks across four categories of VQA: General, Knowledge, OCR & Chart, and Vision-Centric. This provides a broader and more common comparison than prior studies that mainly focus only on vision (Yang et al., 2025c; Fu et al., 2025b) or specialized tasks (Chu et al., 2025).

3.2 Analysis and findings

We compare the performance of MLLMs trained with two post-training approaches across different model scales. First, Figure 2 reports results as the vision model, SigLIP2, scales from 86M to 1B, with the language model fixed to Qwen2.5-3B. Next, Figure 3 shows performances as the language model size increases from 0.5B to 7B, while keeping the vision encoder fixed to SigLIP2-So/16.

Before comparing SFT and DPO, we analyze the impacts of model scaling on MLLM benchmarks. As shown in Figure 2, the performance improves with the size of the vision encoder, confirming the importance of the visual representation capacity within MLLMs. Replacing SigLIP2-B/16 with SigLIP2-g/16 encoder yields significantly better performance on strongly vision-related tasks. For the DPO-tuned MLLM, the gap between the B/16 and g/16 models reaches +4.5%p in Vision-Centric and strikingly +10.6%p in OCR & Chart VQA. In contrast, the improvement is relatively minor at +1.9%p in the weakly

vision-related task, Knowledge VQA. These results show that the vision model plays a crucial role in vision-related tasks, even though the language model scaling in Figure 3 exhibits a large performance gap.

Finding 1: Increasing the capacity of the vision encoder in MLLMs is particularly important for tasks requiring fine-grained visual understanding.

A central focus of our analysis is the comparative efficacy of DPO and SFT for MLLM post-training. The results in Figure 2 show that DPO achieves superior performance compared to SFT, particularly on tasks that require deep visual comprehension rather than those primarily relying on the LLM's knowledge. For instance, on Knowledge VQA benchmarks such as ScienceQA (Lu et al., 2022) and MathVista (Lu et al., 2023), where models rely on scientific or mathematical backgrounds in LLMs, the improvement is only marginal (*e.g.*, +0.3%p). On the other hand, DPO's superiority becomes evident in strongly vision-related benchmarks like OCR & Chart VQA and Vision Centric VQA, including ChartQA (Masry et al., 2022), DocVQA (Mathew et al., 2021), MMVP (Tong et al., 2024b), and CV-bench (Tong et al., 2024a). Quantitatively, with the SigLIP2-L/16, DPO builds a model with +4.2%p and +2.4%p higher performance on OCR & Chart VQA and Vision-Centric VQA, respectively.

The trend of DPO's superiority holds firm even when scaling the language model, as shown in Figure 3. Even as the language model's size increases, the DPO-tuned MLLM consistently surpasses the SFT model, maintaining significant gaps of +3.1%p in OCR & Chart VQA and +4.2%p in Vision-Centric VQA with SigLIP2-g/16. It highlights the superiority of DPO, particularly on tasks requiring detailed visual understanding, and further implies that preference alignment impacts the model's visual processing capabilities, beyond the language model. This observation motivates an in-depth analysis of visual representation in MLLMs.

Finding 2: Preference alignment (DPO) produces MLLMs with superior performance to SFT, especially on strongly vision-related tasks.

As a final analysis, we investigate the effect of data scaling on the *Stage 2* post-training. The training data is scaled from 3K to 40K, whereas the model sizes are fixed to Qwen2.5-1.5B and SigLIP2-So/16. The results are shown in Figure 4. While SFT's performance improves gradually with more data, DPO achieves high performance rapidly, even with a small number of samples. We also observe that a DPO-trained model outperforms an SFT-trained counterpart even with a data disadvantage. For example, DPO with 3K samples achieves a score of 60.4%p, surpassing the 59.5%p score of an SFT model trained on 40K samples. Additional results, including performance on distinct domains, are in Section C.1.

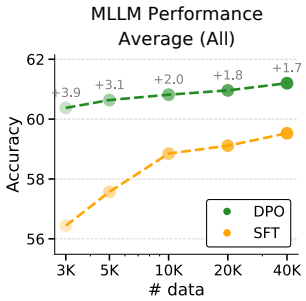


Figure 4 Impact of data scales on MLLM tasks.

4 How does MLLM training affect visual representations?

The previous section demonstrates DPO's superiority over SFT on MLLM benchmarks, with impressive gains on vision-related tasks. The finding suggests that DPO impacts not only the language module but also the model's visual processing capabilities. Several studies have investigated the vision encoder in MLLMs, focusing primarily on architectural adjustments such as enabling vision encoder updates (Bai et al., 2025; Li et al., 2024b), applying all image grids (Li et al., 2025a; Marafioti et al., 2025), and utilizing multiple vision encoders (Tong et al., 2024b,a). In this section, we move beyond these approaches to conduct a deeper analysis of the vision encoder within MLLMs. To the best of our knowledge, this is the first work to conduct an in-depth analysis of the vision encoder in MLLMs.

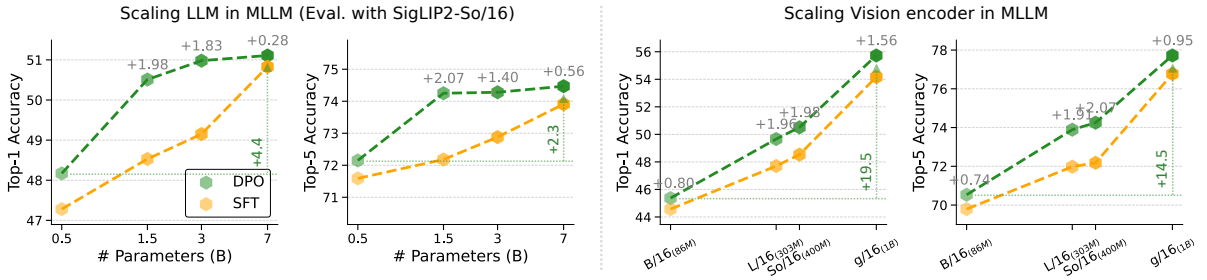


Figure 6 ImageNet accuracy of vision encoder. MLLM post-training is conducted with either SFT or DPO, then the vision encoder is detached from LLM and its vision-only performance evaluated via linear probing. We scale the LLM with a fixed SigLIP2-So/16 (left), or the vision encoder with a fixed Qwen2.5-1.5B (right).

4.1 Experimental setup

We begin with the MLLMs used in Section 3, which are trained with *Stage 1* pre-training and either SFT or DPO *Stage 2* post-training. After separating the vision components from the MLLM (*i.e.*, detaching the vision encoder and projector), we assess their standalone performance on classic vision tasks, including ImageNet classification and semantic segmentation. Performance is measured using image features generated from the vision encoder, or from the combined encoder-projector. In this analysis, we disentangle the impact on the visual representations by isolating the vision encoder from the LLM. More details are available in Section E and the source code.

4.2 Evaluating vision encoders beyond MLLM Benchmarks

ImageNet Classification. We conduct model scaling experiments on ImageNet classification, performing a linear-probe evaluation with the features extracted from the visual components. Note that the features are originally used as the visual token inputs in the MLLM. As shown in Figure 6, our investigation highlights the following key points. (*i*) The MLLM post-training actually reshapes the visual representations. (*ii*) DPO consistently outperforms SFT in the vision-only benchmark, improving ImageNet Top-1 accuracy by +1.83%p for SigLIP2-So/16 coupled with a Qwen-3B head and by +1.96%p for SigLIP2-L/16 with a Qwen-1.5B head. We claim this as a novel finding: DPO—a prevalent RL method in the LLM community (Yang et al., 2025b; Dubey et al., 2024)—is more effective than SFT, not only for **aligning LLMs** but also for **learning visual representations**. (*iii*) MLLM training with larger LLMs yields a high-performing vision encoder. For instance, when trained on DPO, the SigLIP2-So/16 coupled with a 7B LLM exhibits a +4.4%p increase in ImageNet accuracy compared to when coupled with a 0.5B LLM. It supports the hypothesis that larger-capacity LLMs provide more informative optimization signals to the vision encoder.

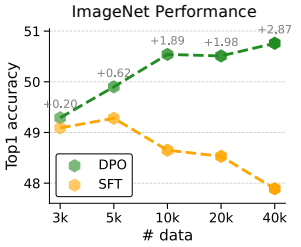


Figure 5 Impact of data scales on ImageNet.

Additionally, we investigate how the data scale of *Stage 2* post-training affects visual representations, using the MLLM architecture described in Section 3 (Qwen2.5-1.5B and SigLIP2-So/16). The results in Figure 5 show a notable difference from those observed in Figure 4. While performance on MLLM benchmarks improves for both SFT and DPO with more data, only DPO benefits from data scaling in the quality of visual representation. This finding suggests that the choice of MLLM training strategy fundamentally alters *how the model sees an image.*

Finding 3: MLLM training not only adapts the language model but also reshapes the visual representations that determine how the model sees an image.

Gradient Visualization. To understand DPO's effectiveness on vision, we investigate how the gradient signals from DPO to the vision encoder differ from those of SFT during the post-training stage. We use Grad-CAM (Selvaraju et al., 2017): we compute the loss for a specific sample x_i as defined in Equation (1)

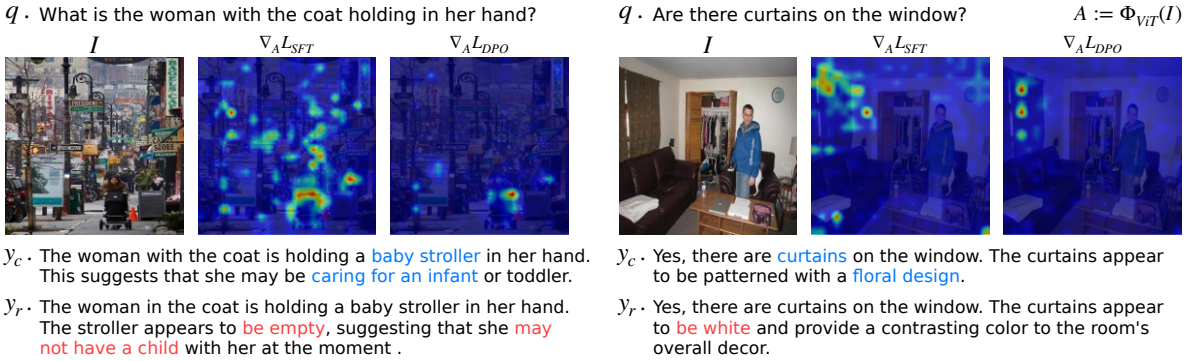


Figure 7 Gradient visualization. Using Grad-CAM (Selvaraju et al., 2017), we visualize the gradient signals received by the vision encoder features ($A := \Phi_{VE}(I)$) under MLLM post-training strategies. We observe that the gradient signals from DPO align more strongly with question-relevant regions than those from SFT.

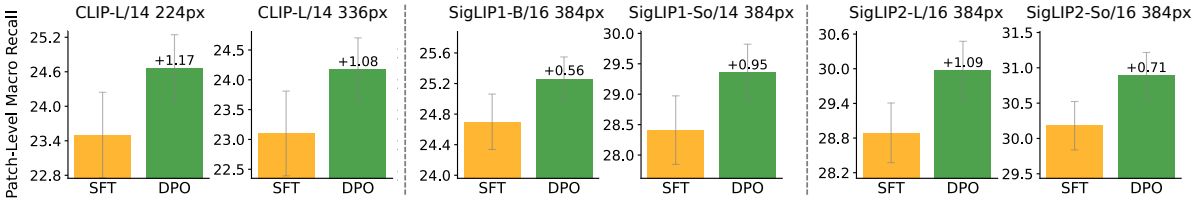


Figure 8 Segmentation probing results. We evaluate segmentation performance via two-layer MLP probing across 6 encoders, each MLLM-trained with a Qwen2.5-1.5B LLM head. The y-axis shows the mean patch-level recall over six random seeds. DPO consistently outperforms over SFT, with the gain shown above the DPO bar.

and perform a backward pass with the sample loss. During the backward pass, we obtain the gradients with respect to the feature activations of the vision encoder, measure the gradient magnitude of each token, and visualize the results. Interestingly, as shown in Figure 7, large gradients primarily occur in question-relevant regions, supporting **Finding 3**. Moreover, the SFT signal tends to be scattered, while the signal from DPO is precisely focused on semantically relevant regions. We hypothesize that the contrastive nature of the DPO objective enables fine-grained gradient signals for the visual representations when differentiating between chosen and rejected responses. Additional results are available in Section C.4.

Image Segmentation. Assuming that DPO enhances the fine-grained training of visual representations, we expect it to be connected with improved localization ability. To measure the localization ability, we perform segmentation probing evaluation with the ADE20K (Zhou et al., 2017) dataset, following the protocol of Covert et al. (2025). First, we utilize MLLM-tuned vision encoders from Section 3. Then, we freeze the vision encoder and attach a two-layer MLP, training it as a patch-level classifier for segmentation. We utilize various vision encoders, based on CLIP (Radford et al., 2021), SigLIP1 (Zhai et al., 2023), and SigLIP2 (Tschannen et al., 2025), all of which are tuned with either SFT or DPO using a Qwen-1.5B LLM. The results in Figure 8 show that the MLLM-tuned vision encoder with DPO consistently outperforms those with SFT on segmentation tasks; for example, DPO-tuned yields a 1.08%p increase in patch-level recall when using a CLIP-L/14 336px encoder. The superiority of DPO is also supported by the qualitative results in Figure 9 and Figure F, showing DPO-tuned vision encoders generate segmentation maps with closer alignment with the ground truth.

Finding 4: DPO steers the vision encoder toward a more fine-grained analysis of visual information, improving its object localization capabilities.

Vision & Language alignment. Huh et al. (2024) proposed a representation alignment metric to evaluate representation similarity between models trained on different modalities, such as vision and language; typically, larger and stronger vision models show higher alignment with LLMs. We adopt this metric to evaluate the representations of a vision encoder. As shown in Figure 10, vision encoders trained with

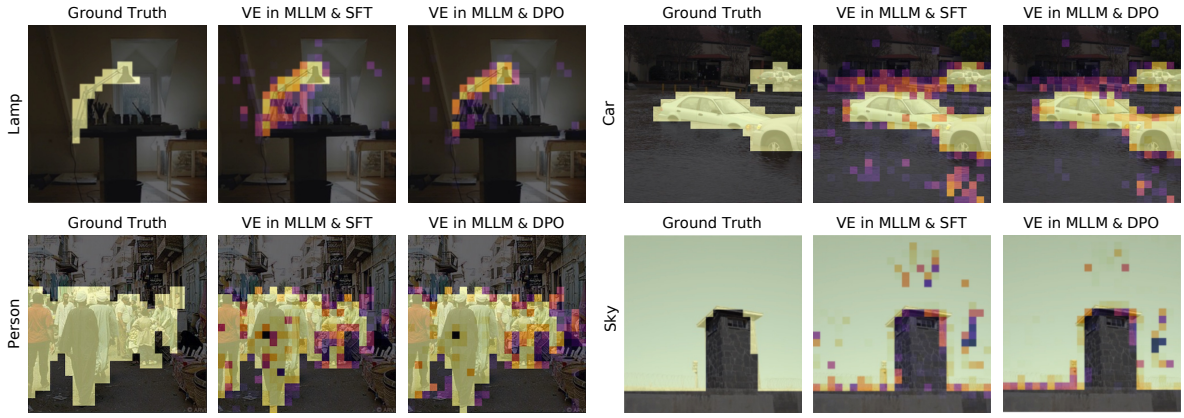


Figure 9 Qualitative results of segmentation. We visualize results from probing on the CLIP-L/14 336px encoder, post-trained with SFT and DPO in MLLMs. The DPO-trained vision encoder (VE) yields more accurate segmentation maps that closely align with the ground truth. More results are in Figure F.

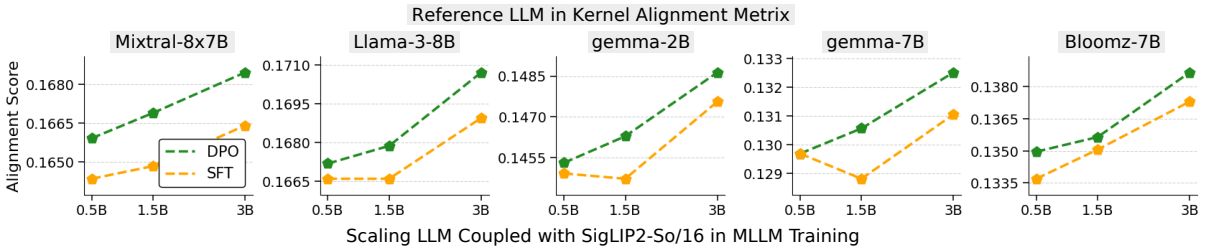


Figure 10 Representational alignment. We measure alignment (Huh et al., 2024) between reference LLMs and vision encoders trained within MLLMs. SigLIP2-So/16, paired with three different LLM scales (x-axis), is trained with DPO or SFT and then used to compute alignment scores against five reference LLMs.

DPO show stronger alignment scores. Additionally, pairing with a larger LLM leads to consistently higher alignment scores, which supports our aforementioned hypothesis that larger LLMs transmit more useful signals to the vision encoder during backpropagation.

Finding 5: The vision encoder benefits from a larger LLM, which provides more informative backward signals for visual representation within an MLLM.

5 Does RL's advantage hold beyond DPO?

Our analyses in Sections 3 and 4 focus on DPO as the representative RL algorithm, chosen for its simplicity and the ease of constructing a controlled comparison with SFT (Section 3.1). A natural question is whether the observed advantages of RL extend to other algorithms. To answer this, we conduct an additional experiment with GRPO (Shao et al., 2024), a reward-model-free RL method that has gained traction in recent LLM and MLLM training (Yang et al., 2025a; Shen et al., 2025).

Setup. We adopt the VLM-R1 codebase (Shen et al., 2025) and train QwenVL-2.5-3B for 1,500 post-training steps with both GRPO and SFT separately, keeping all other configurations identical. Following our evaluation protocol, we measure performance on both VL benchmarks and vision-only benchmarks (*i.e.*, ImageNet classification and segmentation probing).

Results. The results are summarized in Table 1. GRPO outperforms SFT across all evaluated dimensions: it achieves +3.1%p higher average MLLM score, with the largest gain on OCR & Chart (+4.3%p) and Vision-Centric (+3.4%p) tasks, consistent with the DPO trends reported in Section 3. In the vision-only evaluation, the encoder from the GRPO-trained MLLM also yields stronger representations (+1.93%p on ImageNet, +1.83%p on segmentation), echoing our findings in Section 4 that RL reshapes the vision

		MLLM benchmarks					Vision-only	
Model	Post-train	Avg (All)	General	OCR&Chart	Vision	Knowledge	ImageNet	Segment.
QwenVL-2.5-3B	SFT	62.8	69.4	69.0	58.0	55.0	52.01	33.71
QwenVL-2.5-3B	GRPO	**65.9**	**72.1**	**73.3**	**61.4**	**56.7**	**53.94**	**35.54**
	Δ	+3.1	+2.7	+4.3	+3.4	+1.7	+1.93	+1.83

Table 1 GRPO vs. SFT. We extend our analysis beyond DPO by evaluating GRPO. GRPO consistently outperforms SFT on both MLLM benchmarks and vision-only evaluations (*i.e.*, ImageNet classification and segmentation probing), corroborating that the RL advantage over SFT generalizes across different RL methods.

encoder more effectively than SFT. These results confirm that the benefits of RL over SFT are not specific to DPO but generalize to other RL formulations. We provide extended experiments with PPO and MPO, along with further details, in Section B.1.

6 What's next: Unlocking vision model potential via RL

Our analysis has shown that training a vision model with an LLM via DPO builds more fine-grained visual representations than SFT. We now reframe this training process into an effective strategy for evolving vision models, which we term Preference-Instructed Vision OpTimization (PIVOT). In this section, we apply PIVOT to existing vision models that are widely adopted as vision encoders in MLLMs. These include encoders pretrained with image-language supervision[4] (*e.g.*, CLIP and SigLIP) or with vision-only self-supervision (*e.g.*, MAE (He et al., 2022) and DINOv2 (Oquab et al., 2024)). Our objective is to investigate how much these vision models can be improved by PIVOT for use in MLLM.

6.1 Experimental setup

The process begins with a vision encoder commonly used in MLLMs, such as CLIP and SigLIP1. The encoder is attached to an LLM and optimized through both pre-training and post-training with DPO or SFT—on 3M instruction-following samples and 20K preference pairs, as described in Section 3.1. We refer to this training procedure as PIVOT. Afterward, the vision encoder is detached from the LLM, its weights are frozen, and the resulting model is termed the PIVOT-enhanced encoder. We evaluate the performance of PIVOT-enhanced encoder by combining it with Qwen2.5-1.5B to build an MLLM. The combined model is optimized with projector-only pretraining on LAION/CC/SBU-558K (Liu et al., 2024a), followed by instruction finetuning of the projector and LLM on Cambrian's 737K dataset. This design allows us to isolate the encoder's capability and assess the effectiveness of PIVOT representations within MLLMs. Note that we follow the same evaluation protocol as prior works such as Cambrian (Tong et al., 2024a), DINO-MLLM (Fan et al., 2025), and MLLM-data (Han et al., 2025), which has been demonstrated to allow us to study visual representations efficiently. More details are in Section E.7.

6.2 Results

The results are presented in Table 2. In the following, we describe the main comparisons in detail.

SigLIP1 → SigLIP2. We compare an MLLM using the original SigLIP2 encoder with a PIVOT-enhanced SigLIP1. SigLIP2 is a more recent model, developed with substantially larger datasets and an advanced training scheme compared to its predecessor. An MLLM leveraging the SigLIP2-So/16 encoder achieves an average VQA score of 52.4%p. However, by enhancing SigLIP1-So/14 with the PIVOT process, we obtain an MLLM that achieves an average VQA score of 53.2%p, surpassing those with SigLIP2-So/16.

SigLIP2-So/16 → SigLIP2-g/16. SigLIP2-g/16 is considered to have the strongest representations in its family due to its large scale. We compare its MLLM performance against a PIVOT-enhanced SigLIP2-So/16. Despite having 2.5 times fewer parameters, the So/16 model outperforms the g/16 model, achieving a score of 55.6%p versus 53.9%p. This shows the considerable potential for enhancing popular vision backbones for optimal performance within MLLMs.

[4]Following Cambrian (Tong et al., 2024a), we consider CLIP training as strongly supervised, as language provides richer supervision than class labels.

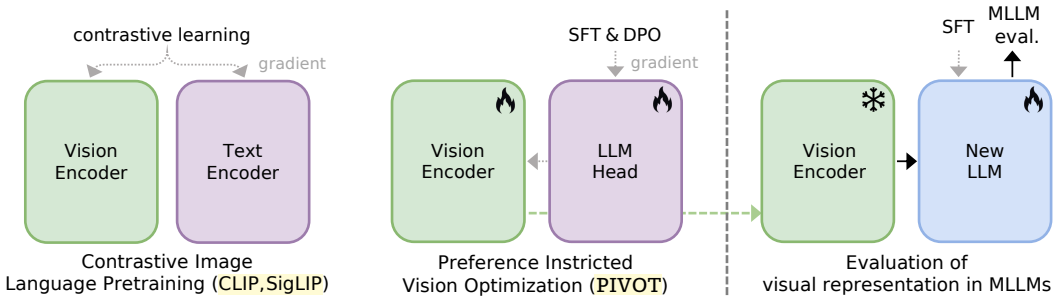


Figure 11 Comparing CLIP and PIVOT training & evaluation of visual representations in MLLMs. CLIP jointly optimizes the vision and text encoders via a contrastive objective, whereas PIVOT trains the vision encoder with an LLM head through SFT and DPO. To evaluate the resulting visual representations, the PIVOT-enhanced encoder is frozen and coupled with a new LLM, following the evaluation protocol of previous works (Tong et al., 2024a; Fan et al., 2025; Han et al., 2025). This setup enables direct assessment of the standalone usefulness of the learned visual representations within MLLMs.

DPO vs. SFT on PIVOT. In Section 4, we show that DPO during post-training benefits even vision encoders within MLLM. Similarly, a vision encoder enhanced by DPO (*i.e.*, PIVOT) provides a 1.3%p advantage over one enhanced with SFT (56.7%p vs. 55.4%p) in the MLLM application when using SigLIP2-g/16. Here, SFT can be seen as similar to the language alignment of (Bolya et al., 2025). This result indicates that DPO's advantage over SFT continues in the context of PIVOT. Thus, we adopt DPO as the default choice for PIVOT.

Classic vision encoders + PIVOT. We investigate the effect of PIVOT on diverse vision encoders and find that all five models improve MLLM performance. An interesting observation is that this improvement holds not only for vision-only self-supervised models such as MAE (He et al., 2022) and MOCO (He et al., 2020), but also for the supervised encoder (Dosovitskiy et al., 2021) trained solely with an image classification loss on the ImageNet dataset.

Model ensemble. The idea of model ensemble utilizing multiple vision encoders for a single MLLM has been explored in prior works (Tong et al., 2024b,a). The experiments show that combining SigLIP1-So/14 and ConvNeXt-XXL increases the average score from 50.9%p to 51.4%p, although it requires a greater number of parameters. We show that SigLIP1-So/14+ PIVOT alone achieves a superior score of 53.2%p without increasing parameters. Furthermore, combining this SigLIP1+ PIVOT with ConvNeXt-XXL results in an additional performance gain, reaching a score of 53.6%p.

Finding 6: Existing vision models possess substantial potential for improvement within MLLMs, which can be unlocked by PIVOT.

We provide additional experimental results in Section B.7, including the impact of training data scale and different usage strategies for the PIVOT-enhanced projector.

6.3 Importance of PIVOT

The idea of PIVOT is simple yet effective: training vision models with an LLM-head using DPO. We highlight the contributions of PIVOT:

1. Positioning PIVOT *not* as a new method, but as an under-explored training regime.
2. Showing that it can develop significantly better MLLMs than those using original vision models, revealing that even state-of-the-art encoders such as SigLIP2, despite large-scale pre-training, retain substantial room for improvement within MLLMs.
3. Presenting the first evidence that DPO reshapes visual features with more positive effects than SFT on standard vision benchmarks as well as on multimodal tasks.

While prior work has shown that SFT-based language alignment can benefit visual representations (Bolya

Evolving vision encoder for MLLM applications				MLLM combining the vision encoder with Qwen2.5-1.5B				
Model	Size	# Params	# Samples seen	Avg (All)	General	OCR&Chart	Vision-Cent.	Knowledge
SigLIP 1 (2023)	So400m	400M	30B	50.9	65.4	42.3	49.8	46.0
+ SFT			30B + 0.003B	52.2	66.5	45.2	50.8	46.3
+ PIVOT			30B + 0.003B	**53.2**	**67.7**	**46.8**	**51.7**	**46.6**
SigLIP 2 (2025)	So400m	400M	40B	52.4	66.2	46.6	50.6	46.1
+ SFT			40B + 0.003B	54.6	66.9	52.2	51.7	47.7
+ PIVOT			40B + 0.003B	**55.6**	**68.1**	**53.9**	**52.4**	**48.1**
SigLIP 2 (2025)	giant	1000M	40B	53.9	66.5	50.8	51.9	46.4
+ SFT			40B + 0.003B	55.4	67.4	52.8	53.1	48.5
+ PIVOT			40B + 0.003B	**56.7**	**68.5**	**54.7**	**54.2**	**49.3**
Classical vision encoders								
Model	Size	# Params	# Samples seen	Avg (All)	General	OCR&Chart	Vision-Cent.	Knowledge
CLIP (2021)	large	303M	32B	46.3	62.1	35.1	43.0	45.0
+ PIVOT			32B + 0.003B	**49.5**	**64.6**	**37.8**	**48.6**	**47.1**
DINOv2 (2024)	giant	1000M	2B	40.9	58.4	17.6	45.1	42.6
+ PIVOT			2B + 0.003B	**43.6**	**62.1**	**18.7**	**49.2**	**44.3**
MAE (2022)	huge	632M	2B	36.8	47.6	17.3	40.2	42.0
+ PIVOT			2B + 0.003B	**39.7**	**52.5**	**18.2**	**43.3**	**44.6**
MOCO (2020)	base	86M	1.4B	35.3	42.5	17.1	39.6	42.1
+ PIVOT			1.4B + 0.003B	**37.5**	**47.4**	**17.6**	**41.0**	**44.1**
ImageNetSup (2021)	huge	632M	N/A	35.5	44.6	17.2	38.2	42.1
+ PIVOT			N/A	**37.7**	**47.3**	**18.1**	**40.3**	**45.1**
Model ensemble (Tong et al., 2024b)								
Model			# Params	Avg (All)	General	OCR&Chart	Vision-Cent.	Knowledge
SigLIP 1-So400m+ DINOv2-L			700M	49.4	64.5	41.5	46.5	45.1
SigLIP 1-So400m+ ConvNeXt-XXL			1.25B	51.4	65.9	44.6	49.1	45.9
SigLIP 1-So400m$_{\text{PIVOT}}$ + ConvNeXt-XXL			1.25B	**53.6**	**67.3**	**48.5**	**52.5**	**46.0**

Table 2 Influence of PIVOT on existing vision models. We apply PIVOT to reveal the potential for improving existing vision models for MLLMs. Following the setup in Section 3.1, the vision model is trained with a Qwen2.5-1.5B LLM-head on 3M samples, and then finetuned with either SFT (+ SFT) or DPO (+ PIVOT) on 20K data. '# samples seen' refers to the number of samples used for whole training as in Cherti et al. (2023); Zhai et al. (2023).

et al., 2025), our results demonstrate that RL yields even stronger improvements, opening up a promising direction for exploring diverse RL algorithms for vision encoder development.

7 Conclusion & Broader impacts

In this work, we investigated the differential impacts of SFT and RL on both MLLMs and their vision encoders. Our experiments first demonstrated that DPO, a form of RL, achieves superior MLLM performance over SFT, particularly on tasks requiring detailed visual comprehension. A subsequent, focused analysis of the vision encoder revealed that DPO induces stronger and more localized visual features. We then consolidated these findings into PIVOT, a practical recipe, and validated its efficacy across a diverse range of vision encoders. We hope this research contributes to the broader goal of enabling MLLMs to better perceive and interpret visual information.

Broader impacts. While our findings demonstrate that RL reshapes visual representations and that PIVOT offers a promising recipe for enhancing vision encoders, several avenues remain open. Our comparison could be further strengthened by equalizing the supervision signals between SFT and DPO, for instance by extending SFT to incorporate negative examples. More broadly, we are particularly interested in exploring novel dataset formats designed to better leverage DPO for visual representation learning, and plan to pursue this as future work.

Beyond our main paper, the supplementary material contains additional analyses, including other RL algorithms (PPO and MPO) vs. SFT (Section B.1), more SFT-friendly settings(Section B.4), text-only benchmarks (Section B.6), and PIVOT ablations(Section B.7).

Acknowledgments

We thank NAVER AI Lab for its generous support. We are also grateful to Heejin Do, Hyesong Choi, Taekyung Kim, and Jaehui Hwang for their valuable feedback.

References

Josh Achiam, Steven Adler, Sandhini Agarwal, Lama Ahmad, Ilge Akkaya, Florencia Leoni Aleman, Diogo Almeida, Janko Altenschmidt, Sam Altman, Shyamal Anadkat, et al. Gpt-4 technical report. *arXiv preprint arXiv:2303.08774*, 2023. 1, 20

Mohammad Gheshlaghi Azar, Zhaohan Daniel Guo, Bilal Piot, Remi Munos, Mark Rowland, Michal Valko, and Daniele Calandriello. A general theoretical paradigm to understand learning from human preferences. In *International Conference on Artificial Intelligence and Statistics*. PMLR, 2024. 20

Jinze Bai, Shuai Bai, Yunfei Chu, Zeyu Cui, Kai Dang, Xiaodong Deng, Yang Fan, Wenbin Ge, Yu Han, Fei Huang, et al. Qwen technical report. *arXiv preprint arXiv:2309.16609*, 2023a. 20, 32

Jinze Bai, Shuai Bai, Shusheng Yang, Shijie Wang, Sinan Tan, Peng Wang, Junyang Lin, Chang Zhou, and Jingren Zhou. Qwen-vl: A versatile vision-language model for understanding, localization, text reading, and beyond. *arXiv preprint arXiv:2308.12966*, 2023b. 1, 20

Shuai Bai, Keqin Chen, Xuejing Liu, Jialin Wang, Wenbin Ge, Sibo Song, Kai Dang, Peng Wang, Shijie Wang, Jun Tang, et al. Qwen2. 5-vl technical report. *arXiv preprint arXiv:2502.13923*, 2025. 5, 20

Hangbo Bao, Li Dong, Songhao Piao, and Furu Wei. Beit: Bert pre-training of image transformers. In *ICLR*, 2022. 20

Daniel Bolya, Po-Yao Huang, Peize Sun, Jang Hyun Cho, Andrea Madotto, Chen Wei, Tengyu Ma, Jiale Zhi, Jathushan Rajasegaran, Hanoona Rasheed, Junke Wang, Marco Monteiro, Hu Xu, Shiyu Dong, Nikhila Ravi, Daniel Li, Piotr Dollár, and Christoph Feichtenhofer. Perception encoder: The best visual embeddings are not at the output of the network, 2025. URL https://arxiv.org/abs/2504.13181. 10, 21

Tom Brown, Benjamin Mann, Nick Ryder, Melanie Subbiah, Jared D Kaplan, Prafulla Dhariwal, Arvind Neelakantan, Pranav Shyam, Girish Sastry, Amanda Askell, et al. Language models are few-shot learners. *NeurIPS*, 2020. 1, 2, 20

Mathilde Caron, Ishan Misra, Julien Mairal, Priya Goyal, Piotr Bojanowski, and Armand Joulin. Unsupervised learning of visual features by contrasting cluster assignments. In *NeurIPS*, 2020. 20

Mathilde Caron, Hugo Touvron, Ishan Misra, Hervé Jégou, Julien Mairal, Piotr Bojanowski, and Armand Joulin. Emerging properties in self-supervised vision transformers. In *ICCV*, 2021. 20

Liang Chen, Lei Li, Haozhe Zhao, Yifan Song, and Vinci. R1-v: Reinforcing super generalization ability in vision-language models with less than $3. https://github.com/Deep-Agent/R1-V, 2025. 22

Ting Chen, Simon Kornblith, Mohammad Norouzi, and Geoffrey Hinton. A simple framework for contrastive learning of visual representations. In *ICML*, 2020. 20

Xinlei Chen and Kaiming He. Exploring simple siamese representation learning. In *CVPR*, 2021. 20

Xinlei Chen, Hao Fang, Tsung-Yi Lin, Ramakrishna Vedantam, Saurabh Gupta, Piotr Dollár, and C Lawrence Zitnick. Microsoft coco captions: Data collection and evaluation server. *arXiv preprint arXiv:1504.00325*, 2015. 25

Zhe Chen, Jiannan Wu, Wenhai Wang, Weijie Su, Guo Chen, Sen Xing, Muyan Zhong, Qinglong Zhang, Xizhou Zhu, Lewei Lu, et al. Internvl: Scaling up vision foundation models and aligning for generic visual-linguistic tasks. In *CVPR*, 2024. 1, 32

Mehdi Cherti, Romain Beaumont, Ross Wightman, Mitchell Wortsman, Gabriel Ilharco, Cade Gordon, Christoph Schuhmann, Ludwig Schmidt, and Jenia Jitsev. Reproducible scaling laws for contrastive language-image learning. In *CVPR*, 2023. 11

Paul F Christiano, Jan Leike, Tom Brown, Miljan Martic, Shane Legg, and Dario Amodei. Deep reinforcement learning from human preferences. In *NeuIPS*, 2017. 1, 2, 20

Tianzhe Chu, Yuexiang Zhai, Jihan Yang, Shengbang Tong, Saining Xie, Dale Schuurmans, Quoc V Le, Sergey Levine, and Yi Ma. Sft memorizes, rl generalizes: A comparative study of foundation model post-training. In *ICML*, 2025. 3, 4, 20, 21, 22, 23, 24

Karl Cobbe, Vineet Kosaraju, Mohammad Bavarian, Mark Chen, Heewoo Jun, Lukasz Kaiser, Matthias Plappert, Jerry Tworek, Jacob Hilton, Reiichiro Nakano, et al. Training verifiers to solve math word problems. *arXiv preprint arXiv:2110.14168*, 2021. 25, 26

Ian Covert, Tony Sun, James Zou, and Tatsunori Hashimoto. Locality alignment improves vision-language models. In *ICLR*, 2025. 7, 35

Zihang Dai, Zhilin Yang, Yiming Yang, Jaime Carbonell, Quoc V Le, and Ruslan Salakhutdinov. Transformer-xl: Attentive language models beyond a fixed-length context. In *ACL*, 2019. 2, 20

Jacob Devlin, Ming-Wei Chang, Kenton Lee, and Kristina Toutanova. Bert: Pre-training of deep bidirectional transformers for language understanding. In *Proceedings of the 2019 conference of the North American chapter of the association for computational linguistics: human language technologies, volume 1 (long and short papers)*, 2019. 20

Hongyuan Dong, Jiawen Li, Bohong Wu, Jiacong Wang, Yuan Zhang, and Haoyuan Guo. Benchmarking and improving detail image caption. *arXiv preprint arXiv:2405.19092*, 2024. 25

Alexey Dosovitskiy, Lucas Beyer, Alexander Kolesnikov, Dirk Weissenborn, Xiaohua Zhai, Thomas Unterthiner, Mostafa Dehghani, Matthias Minderer, Georg Heigold, Sylvain Gelly, et al. An image is worth 16x16 words: Transformers for image recognition at scale. In *ICLR*, 2021. 10, 11

Danny Driess, Fei Xia, Mehdi SM Sajjadi, Corey Lynch, Aakanksha Chowdhery, Ayzaan Wahid, Jonathan Tompson, Quan Vuong, Tianhe Yu, Wenlong Huang, et al. Palm-e: An embodied multimodal language model. In *ICML*, 2023. 2

Abhimanyu Dubey, Abhinav Jauhri, Abhinav Pandey, Abhishek Kadian, Ahmad Al-Dahle, Aiesha Letman, Akhil Mathur, Alan Schelten, Amy Yang, Angela Fan, et al. The llama 3 herd of models. *arXiv e-prints*, pp. arXiv–2407, 2024. 1, 3, 6, 32, 35

Kawin Ethayarajh, Winnie Xu, Niklas Muennighoff, Dan Jurafsky, and Douwe Kiela. Kto: Model alignment as prospect theoretic optimization. In *ICML*, 2024. 20

David Fan, Shengbang Tong, Jiachen Zhu, Koustuv Sinha, Zhuang Liu, Xinlei Chen, Michael Rabbat, Nicolas Ballas, Yann LeCun, Amir Bar, et al. Scaling language-free visual representation learning. In *ICCV*, 2025. 1, 9, 10, 27, 31, 35

Chaoyou Fu, Peixian Chen, Yunhang Shen, Yulei Qin, Mengdan Zhang, Xu Lin, Zhenyu Qiu, Wei Lin, Jinrui Yang, Xiawu Zheng, et al. Mme: a comprehensive evaluation benchmark for multimodal large language models. corr abs/2306.13394 (2023), 2023. 34

Jinlan Fu, Shenzhen Huangfu, Hao Fei, Xiaoyu Shen, Bryan Hooi, Xipeng Qiu, and See-Kiong Ng. Chip: Cross-modal hierarchical direct preference optimization for multimodal llms. In *ICLR*, 2025a. 2, 3, 20, 21, 31

Yuhan Fu, Ruobing Xie, Xingwu Sun, Zhanhui Kang, and Xirong Li. Mitigating hallucination in multimodal large language model via hallucination-targeted direct preference optimization. In *ACL*, 2025b. 2, 4, 20, 21

Yuying Ge, Yixiao Ge, Ziyun Zeng, Xintao Wang, and Ying Shan. Planting a seed of vision in large language model. *arXiv preprint arXiv:2307.08041*, 2023. 34

Tianrui Guan, Fuxiao Liu, Xiyang Wu, Ruiqi Xian, Zongxia Li, Xiaoyu Liu, Xijun Wang, Lichang Chen, Furong Huang, Yaser Yacoob, et al. Hallusionbench: an advanced diagnostic suite for entangled language hallucination and visual illusion in large vision-language models. In *CVPR*, 2024. 25

Junlin Han, Shengbang Tong, David Fan, Yufan Ren, Koustuv Sinha, Philip Torr, and Filippos Kokkinos. Learning to see before seeing: Demystifying llm visual priors from language pre-training. *arXiv preprint arXiv:2509.26625*, 2025. 9, 10, 20, 27, 31, 35

Kaiming He, Haoqi Fan, Yuxin Wu, Saining Xie, and Ross Girshick. Momentum contrast for unsupervised visual representation learning. In *CVPR*, 2020. 10, 11, 20

Kaiming He, Xinlei Chen, Saining Xie, Yanghao Li, Piotr Dollár, and Ross Girshick. Masked autoencoders are scalable vision learners. In *CVPR*, 2022. 2, 9, 10, 11, 20

Dan Hendrycks, Collin Burns, Steven Basart, Andy Zou, Mantas Mazeika, Dawn Song, and Jacob Steinhardt. Measuring massive multitask language understanding. In *ICLR*, 2021. 25, 26

Tuomo Hiippala, Malihe Alikhani, Jonas Haverinen, Timo Kalliokoski, Evanfiya Logacheva, Serafina Orekhova, Aino Tuomainen, Matthew Stone, and John A Bateman. Ai2d-rst: A multimodal corpus of 1000 primary school science diagrams. *Language Resources and Evaluation*, 55:661–688, 2021. 34

Jiwoo Hong, Noah Lee, and James Thorne. Orpo: Monolithic preference optimization without reference model. *EMNLP*, 2024. 20

Drew A. Hudson and Christopher D. Manning. Gqa: A new dataset for real-world visual reasoning and compositional question answering. In *CVPR*, 2019. 34

Minyoung Huh, Brian Cheung, Tongzhou Wang, and Phillip Isola. The platonic representation hypothesis. In *ICML*, 2024. 7, 8

Andrew Jaegle, Sebastian Borgeaud, Jean-Baptiste Alayrac, Carl Doersch, Catalin Ionescu, David Ding, Skanda Koppula, Daniel Zoran, Andrew Brock, Evan Shelhamer, et al. Perceiver io: A general architecture for structured inputs & outputs. In *ICLR*, 2022. 20

Gueyoung Jung, Matti A Hiltunen, Kaustubh R Joshi, Richard D Schlichting, and Calton Pu. Mistral: Dynamically managing power, performance, and adaptation cost in cloud infrastructures. In *2010 IEEE 30th International Conference on Distributed Computing Systems*, pp. 62–73. IEEE, 2010. 35

Oğuzhan Fatih Kar, Alessio Tonioni, Petra Poklukar, Achin Kulshrestha, Amir Zamir, and Federico Tombari. Brave: Broadening the visual encoding of vision-language models. In *ECCV*, 2024. 20

Siddharth Karamcheti, Suraj Nair, Ashwin Balakrishna, Percy Liang, Thomas Kollar, and Dorsa Sadigh. Prismatic vlms: Investigating the design space of visually-conditioned language models. In *ICML*, 2024. 2

Weixian Lei, Jiacong Wang, Haochen Wang, Xiangtai Li, Jun Hao Liew, Jiashi Feng, and Zilong Huang. The scalability of simplicity: Empirical analysis of vision-language learning with a single transformer. *arXiv preprint arXiv:2504.10462*, 2025. 3

Mike Lewis, Yinhan Liu, Naman Goyal, Marjan Ghazvininejad, Abdelrahman Mohamed, Omer Levy, Ves Stoyanov, and Luke Zettlemoyer. Bart: Denoising sequence-to-sequence pre-training for natural language generation, translation, and comprehension. In *ACL*, 2020. 20

Baiqi Li, Zhiqiu Lin, Wenxuan Peng, Jean de Dieu Nyandwi, Daniel Jiang, Zixian Ma, Simran Khanuja, Ranjay Krishna, Graham Neubig, and Deva Ramanan. Naturalbench: Evaluating vision-language models on natural adversarial samples. In *NeurIPS*, 2024a. 25

Bo Li, Yuanhan Zhang, Dong Guo, Renrui Zhang, Feng Li, Hao Zhang, Kaichen Zhang, Peiyuan Zhang, Yanwei Li, Ziwei Liu, et al. Llava-onevision: Easy visual task transfer. *TMLR*, 2025a. 1, 3, 4, 5, 20, 21, 27, 28, 32

Feng Li, Renrui Zhang, Hao Zhang, Yuanhan Zhang, Bo Li, Wei Li, Zejun Ma, and Chunyuan Li. Llava-next-interleave: Tackling multi-image, video, and 3d in large multimodal models. *arXiv preprint arXiv:2407.07895*, 2024b. 2, 3, 5, 20, 27, 28

Haozhan Li, Yuxin Zuo, Jiale Yu, Yuhao Zhang, Zhaohui Yang, Kaiyan Zhang, Xuekai Zhu, Yuchen Zhang, Tianxing Chen, Ganqu Cui, Dehui Wang, Dingxiang Luo, Yuchen Fan, Youbang Sun, Jia Zeng, Jiangmiao Pang, Shanghang Zhang, Yu Wang, Yao Mu, Bowen Zhou, and Ning Ding. Simplevla-rl: Scaling vla training via reinforcement learning. *arXiv preprint arXiv:2509.09674*, 2025b. 3, 20, 21, 22, 23, 24

Junnan Li, Dongxu Li, Silvio Savarese, and Steven Hoi. Blip-2: Bootstrapping language-image pre-training with frozen image encoders and large language models. In *ICML*, 2023a. 1, 2, 20, 27, 28

Lei Li, Yuancheng Wei, Zhihui Xie, Xuqing Yang, Yifan Song, Peiyi Wang, Chenxin An, Tianyu Liu, Sujian Li, Bill Yuchen Lin, et al. Vl-rewardbench: A challenging benchmark for vision-language generative reward models. In *CVPR*, 2025c. 25

Yifan Li, Yifan Du, Kun Zhou, Jinpeng Wang, Wayne Xin Zhao, and Ji-Rong Wen. Evaluating object hallucination in large vision-language models. In *EMNLP*, 2023b. 25

Yuan-Hong Liao, Sven Elflein, Liu He, Laura Leal-Taixé, Yejin Choi, Sanja Fidler, and David Acuna. Longperceptualthoughts: Distilling system-2 reasoning for system-1 perception. *arXiv preprint arXiv:2504.15362*, 2025. 21, 31

Ziyi Lin, Chris Liu, Renrui Zhang, Peng Gao, Longtian Qiu, Han Xiao, Han Qiu, Chen Lin, Wenqi Shao, Keqin Chen, et al. Sphinx: The joint mixing of weights, tasks, and visual embeddings for multi-modal large language models. In *ECCV*, 2024. 20, 27, 28

Haotian Liu, Chunyuan Li, Qingyang Wu, and Yong Jae Lee. Visual instruction tuning. In *NeurIPS*, 2023a. 1, 2, 20, 22

Haotian Liu, Chunyuan Li, Yuheng Li, and Yong Jae Lee. Improved baselines with visual instruction tuning. In *CVPR*, 2024a. 1, 4, 9, 27

Yuan Liu, Haodong Duan, Yuanhan Zhang, Bo Li, Songyang Zhang, Wangbo Zhao, Yike Yuan, Jiaqi Wang, Conghui He, Ziwei Liu, et al. Mmbench: Is your multi-modal model an all-around player? In *ECCV*, 2024b. 34

Yuliang Liu, Zhang Li, Hongliang Li, Wenwen Yu, Mingxin Huang, Dezhi Peng, Mingyu Liu, Mingrui Chen, Chunyuan Li, Lianwen Jin, et al. On the hidden mystery of ocr in large multimodal models. *arXiv preprint arXiv:2305.07895*, 2023b. 34

Pan Lu, Swaroop Mishra, Tanglin Xia, Liang Qiu, Kai-Wei Chang, Song-Chun Zhu, Oyvind Tafjord, Peter Clark, and Ashwin Kalyan. Learn to explain: Multimodal reasoning via thought chains for science question answering. In *NeurIPS*, 2022. 5, 34

Pan Lu, Hritik Bansal, Tony Xia, Jiacheng Liu, Chunyuan Li, Hannaneh Hajishirzi, Hao Cheng, Kai-Wei Chang, Michel Galley, and Jianfeng Gao. Mathvista: Evaluating mathematical reasoning of foundation models in visual contexts. In *ICLR*, 2023. 5, 34

Andrés Marafioti, Orr Zohar, Miquel Farré, Merve Noyan, Elie Bakouch, Pedro Cuenca, Cyril Zakka, Loubna Ben Allal, Anton Lozhkov, Nouamane Tazi, et al. Smolvlm: Redefining small and efficient multimodal models. *arXiv preprint arXiv:2504.05299*, 2025. 5

Ahmed Masry, Do Xuan Long, Jia Qing Tan, Shafiq Joty, and Enamul Hoque. Chartqa: A benchmark for question answering about charts with visual and logical reasoning. In *ACL*, 2022. 5, 34

Minesh Mathew, Dimosthenis Karatzas, and CV Jawahar. Docvqa: A dataset for vqa on document images. In *WACV*, 2021. 5, 34

Kohsei Matsutani, Shota Takashiro, Gouki Minegishi, Takeshi Kojima, Yusuke Iwasawa, and Yutaka Matsuo. Rl squeezes, sft expands: A comparative study of reasoning llms. *arXiv preprint arXiv:2509.21128*, 2025. 20

Ron Mokady, Amir Hertz, and Amit H Bermano. Clipcap: Clip prefix for image captioning. *arXiv preprint arXiv:2111.09734*, 2021. 1

Niklas Muennighoff, Thomas Wang, Lintang Sutawika, Adam Roberts, Stella Biderman, TL Scao, M Saiful Bari, Sheng Shen, Zheng-Xin Yong, Hailey Schoelkopf, et al. Crosslingual generalization through multitask finetuning (2022). *arXiv preprint arXiv:2211.01786*, 1786. 35

Maxime Oquab, Timothée Darcet, Théo Moutakanni, Huy Vo, Marc Szafraniec, Vasil Khalidov, Pierre Fernandez, Daniel Haziza, Francisco Massa, Alaaeldin El-Nouby, et al. DINOv2: Learning robust visual features without supervision. *TMLR*, 2024. 2, 9, 11

Long Ouyang, Jeffrey Wu, Xu Jiang, Diogo Almeida, Carroll Wainwright, Pamela Mishkin, Chong Zhang, Sandhini Agarwal, Katarina Slama, Alex Ray, et al. Training language models to follow instructions with human feedback. In *NeuIPS*, 2022. 1, 2, 4, 20

Jean Piaget, Margaret Cook, et al. *The origins of intelligence in children*, volume 8. International Universities Press New York, 1952. 1

Alec Radford, Karthik Narasimhan, Tim Salimans, Ilya Sutskever, et al. Improving language understanding by generative pre-training. 2018. 2, 20, 30

Alec Radford, Jong Wook Kim, Chris Hallacy, Aditya Ramesh, Gabriel Goh, Sandhini Agarwal, Girish Sastry, Amanda Askell, Pamela Mishkin, Jack Clark, et al. Learning transferable visual models from natural language supervision. In *ICML*, 2021. 2, 7, 11, 21

Rafael Rafailov, Archit Sharma, Eric Mitchell, Christopher D Manning, Stefano Ermon, and Chelsea Finn. Direct preference optimization: Your language model is secretly a reward model. In *NeuIPS*, 2023. 3, 20, 21, 30

Colin Raffel, Noam Shazeer, Adam Roberts, Katherine Lee, Sharan Narang, Michael Matena, Yanqi Zhou, Wei Li, and Peter J Liu. Exploring the limits of transfer learning with a unified text-to-text transformer. *Journal of machine learning research*, 2020. 20

John Schulman, Filip Wolski, Prafulla Dhariwal, Alec Radford, and Oleg Klimov. Proximal policy optimization algorithms. *arXiv preprint arXiv:1707.06347*, 2017. 20, 21

Ramprasaath R Selvaraju, Michael Cogswell, Abhishek Das, Ramakrishna Vedantam, Devi Parikh, and Dhruv Batra. Grad-cam: Visual explanations from deep networks via gradient-based localization. In *ICCV*, 2017. 6, 7, 36

Zhihong Shao, Peiyi Wang, Qihao Zhu, Runxin Xu, Junxiao Song, Xiao Bi, Haowei Zhang, Mingchuan Zhang, YK Li, Y Wu, et al. Deepseekmath: Pushing the limits of mathematical reasoning in open language models, 2024. *arXiv preprint arXiv:2402.03300*, 2024. 3, 8, 20, 21

Haozhan Shen, Peng Liu, Jingcheng Li, Chunxin Fang, Yibo Ma, Jiajia Liao, Qiaoli Shen, Zilun Zhang, Kangjia Zhao, Qianqian Zhang, Ruochen Xu, and Tiancheng Zhao. Vlm-r1: A stable and generalizable r1-style large vision-language model. *arXiv preprint arXiv:2504.07615*, 2025. 8, 22

Idan Shenfeld, Jyothish Pari, and Pulkit Agrawal. Rl's razor: Why online reinforcement learning forgets less. *arXiv preprint arXiv:2509.04259*, 2025. 20, 23, 24

Mustafa Shukor, Enrico Fini, Victor Guilherme Turrisi da Costa, Matthieu Cord, Joshua Susskind, and Alaaeldin El-Nouby. Scaling laws for native multimodal models. In *ICCV*, 2025. 3

Amanpreet Singh, Vivek Natarajan, Meet Shah, Yu Jiang, Xinlei Chen, Dhruv Batra, Devi Parikh, and Marcus Rohrbach. Towards vqa models that can read. In *CVPR*, 2019. 34

Quan Sun, Yuxin Fang, Ledell Wu, Xinlong Wang, and Yue Cao. Eva-clip: Improved training techniques for clip at scale. *arXiv preprint arXiv:2303.15389*, 2023. 21

Zhiqing Sun, Sheng Shen, Shengcao Cao, Haotian Liu, Chunyuan Li, Yikang Shen, Chuang Gan, Liang-Yan Gui, Yu-Xiong Wang, Yiming Yang, et al. Aligning large multimodal models with factually augmented rlhf. In *ACL*, 2024. 2, 3, 20, 21, 22

Gemini Team, Rohan Anil, Sebastian Borgeaud, Jean-Baptiste Alayrac, Jiahui Yu, Radu Soricut, Johan Schalkwyk, Andrew M Dai, Anja Hauth, Katie Millican, et al. Gemini: a family of highly capable multimodal models. *arXiv preprint arXiv:2312.11805*, 2023. 1

Gemini Team, Petko Georgiev, Ving Ian Lei, Ryan Burnell, Libin Bai, Anmol Gulati, Garrett Tanzer, Damien Vincent, Zhufeng Pan, Shibo Wang, et al. Gemini 1.5: Unlocking multimodal understanding across millions of tokens of context. *arXiv preprint arXiv:2403.05530*, 2024a. 1, 20

Gemma Team, Thomas Mesnard, Cassidy Hardin, Robert Dadashi, Surya Bhupatiraju, Shreya Pathak, Laurent Sifre, Morgane Rivière, Mihir Sanjay Kale, Juliette Love, et al. Gemma: Open models based on gemini research and technology. *arXiv preprint arXiv:2403.08295*, 2024b. 32, 35

Peter Tong, Ellis Brown, Penghao Wu, Sanghyun Woo, Adithya Jairam Vedagiri IYER, Sai Charitha Akula, Shusheng Yang, Jihan Yang, Manoj Middepogu, Ziteng Wang, et al. Cambrian-1: A fully open, vision-centric exploration of multimodal llms. *NeurIPS*, 2024a. 1, 2, 3, 5, 9, 10, 20, 27, 31, 34, 35

Shengbang Tong, Zhuang Liu, Yuexiang Zhai, Yi Ma, Yann LeCun, and Saining Xie. Eyes wide shut? exploring the visual shortcomings of multimodal llms. In *CVPR*, 2024b. 1, 5, 10, 11, 20, 34

Hugo Touvron, Thibaut Lavril, Gautier Izacard, Xavier Martinet, Marie-Anne Lachaux, Timothée Lacroix, Baptiste Rozière, Naman Goyal, Eric Hambro, Faisal Azhar, et al. Llama: Open and efficient foundation language models. *arXiv preprint arXiv:2302.13971*, 2023a. 20, 30

Hugo Touvron, Louis Martin, Kevin Stone, Peter Albert, Amjad Almahairi, Yasmine Babaei, Nikolay Bashlykov, Soumya Batra, Prajjwal Bhargava, Shruti Bhosale, et al. Llama 2: Open foundation and fine-tuned chat models. *arXiv preprint arXiv:2307.09288*, 2023b. 2, 20

Michael Tschannen, Alexey Gritsenko, Xiao Wang, Muhammad Ferjad Naeem, Ibrahim Alabdulmohsin, Nikhil Parthasarathy, Talfan Evans, Lucas Beyer, Ye Xia, Basil Mustafa, et al. Siglip 2: Multilingual vision-language encoders with improved semantic understanding, localization, and dense features. *arXiv preprint arXiv:2502.14786*, 2025. 3, 7, 11, 21

Fei Wang, Wenxuan Zhou, James Y Huang, Nan Xu, Sheng Zhang, Hoifung Poon, and Muhao Chen. mdpo: Conditional preference optimization for multimodal large language models. In *EMNLP*, 2024a. 2, 3, 20, 21, 31

Weiyun Wang, Zhe Chen, Wenhai Wang, Yue Cao, Yangzhou Liu, Zhangwei Gao, Jinguo Zhu, Xizhou Zhu, Lewei Lu, Yu Qiao, et al. Enhancing the reasoning ability of multimodal large language models via mixed preference optimization. *arXiv preprint arXiv:2411.10442*, 2024b. 2, 3, 4, 20, 21, 22, 24, 25, 31, 33

xAI. grok, 2024. URL https://x.ai/blog/grok-1.5v. 34

Yuxi Xie, Guanzhen Li, Xiao Xu, and Min-Yen Kan. V-dpo: Mitigating hallucination in large vision language models via vision-guided direct preference optimization. In *EMNLP*, 2024. 20, 21

Tianyi Xiong, Xiyao Wang, Dong Guo, Qinghao Ye, Haoqi Fan, Quanquan Gu, Heng Huang, and Chunyuan Li. Llava-critic: Learning to evaluate multimodal models. In *CVPR*, 2025. 20, 21

An Yang, Anfeng Li, Baosong Yang, Beichen Zhang, Binyuan Hui, Bo Zheng, Bowen Yu, Chang Gao, Chengen Huang, Chenxu Lv, et al. Qwen2.5 technical report. *arXiv preprint arXiv:2412.15115*, 2025a. 3, 8, 32

An Yang, Anfeng Li, Baosong Yang, Beichen Zhang, Binyuan Hui, Bo Zheng, Bowen Yu, Chang Gao, Chengen Huang, Chenxu Lv, et al. Qwen3 technical report. *arXiv preprint arXiv:2505.09388*, 2025b. 1, 6

Zhihe Yang, Xufang Luo, Dongqi Han, Yunjian Xu, and Dongsheng Li. Mitigating hallucinations in large vision-language models via dpo: On-policy data hold the key. In *CVPR*, 2025c. 2, 3, 4, 20, 21

Zhilin Yang, Zihang Dai, Yiming Yang, Jaime Carbonell, Russ R Salakhutdinov, and Quoc V Le. Xlnet: Generalized autoregressive pretraining for language understanding. In *NeurIPS*, 2019. 2

Tianyu Yu, Yuan Yao, Haoye Zhang, Taiwen He, Yifeng Han, Ganqu Cui, Jinyi Hu, Zhiyuan Liu, Hai-Tao Zheng, Maosong Sun, et al. Rlhf-v: Towards trustworthy mllms via behavior alignment from fine-grained correctional human feedback. In *CVPR*, 2024. 2, 3, 4, 21, 31

Tianyu Yu, Haoye Zhang, Qiming Li, Qixin Xu, Yuan Yao, Da Chen, Xiaoman Lu, Ganqu Cui, Yunkai Dang, Taiwen He, et al. Rlaif-v: Open-source ai feedback leads to super gpt-4v trustworthiness. In *CVPR*, 2025. 3, 20, 21, 31

Xiang Yue, Yuansheng Ni, Kai Zhang, Tianyu Zheng, Ruoqi Liu, Ge Zhang, Samuel Stevens, Dongfu Jiang, Weiming Ren, Yuxuan Sun, et al. Mmmu: A massive multi-discipline multimodal understanding and reasoning benchmark for expert agi. In *CVPR*, 2024. 34

Fatemeh Pesaran Zadeh, Yoojin Oh, and Gunhee Kim. Lpoi: Listwise preference optimization for vision language models. In *ACL*, 2025. 20, 21

Rowan Zellers, Ari Holtzman, Yonatan Bisk, Ali Farhadi, and Yejin Choi. Hellaswag: Can a machine really finish your sentence? In *ACL*, 2019. 25, 26

Xiaohua Zhai, Basil Mustafa, Alexander Kolesnikov, and Lucas Beyer. Sigmoid loss for language image pre-training. In *ICCV*, 2023. 7, 11, 21

Yuexiang Zhai, Hao Bai, Zipeng Lin, Jiayi Pan, Shengbang Tong, Yifei Zhou, Alane Suhr, Saining Xie, Yann LeCun, Yi Ma, and Sergey Levine. Fine-tuning large vision-language models as decision-making agents via reinforcement learning. In *NeruIPS*, 2024. 22

Kaichen Zhang, Bo Li, Peiyuan Zhang, Fanyi Pu, Joshua Adrian Cahyono, Kairui Hu, Shuai Liu, Yuanhan Zhang, Jingkang Yang, Chunyuan Li, and Ziwei Liu. Lmms-eval: Reality check on the evaluation of large multimodal models, 2024. URL https://arxiv.org/abs/2407.12772. 34

Yi-Fan Zhang, Huanyu Zhang, Haochen Tian, Chaoyou Fu, Shuangqing Zhang, Junfei Wu, Feng Li, Kun Wang, Qingsong Wen, Zhang Zhang, et al. Mme-realworld: Could your multimodal llm challenge high-resolution real-world scenarios that are difficult for humans? In *ICLR*, 2025. 25

Yaowei Zheng, Junting Lu, Shenzhi Wang, Zhangchi Feng, Dongdong Kuang, and Yuwen Xiong. Easyr1: An efficient, scalable, multi-modality rl training framework. https://github.com/hiyouga/EasyR1, 2025. 22

Bolei Zhou, Hang Zhao, Xavier Puig, Sanja Fidler, Adela Barriuso, and Antonio Torralba. Scene parsing through ade20k dataset. In *CVPR*, 2017. 7, 35

Appendix

Table of Contents

A Related Work **20**

A.1 MLLMs. 20

A.2 LLMs with RL. 20

A.3 MLLMs with RL 20

A.4 Vision-centric pre-trainings 20

B Additional Experiments **21**

B.1 Other RL algorithms vs. SFT 21

B.2 MLLM Training Sensitivity 23

B.3 MLLM performance under new data distributions 23

B.4 MLLM performance under more SFT-friendly data 24

B.5 MLLM performance on hallucination, captioning, and robustness benchmarks 25

B.6 MLLM performance on text-only benchmarks 25

B.7 PIVOT ablation study 26

B.8 PIVOT performance comparison with existing MLLMs 27

C Extended Results from the Main Paper **27**

C.1 MLLM training data scaling 27

C.2 Performance of MLLMs on all 16 benchmarks 28

C.3 ImageNet classification with a vision encoder 28

C.4 Gradient visualization of a vision encoder 29

C.5 Segmentation probing with a vision encoder 29

D Discussions **30**

D.1 Understanding SFT and DPO 30

D.2 Low performance gap on Knowledge VQA 30

D.3 Positioning our work within RL-based MLLM research 31

D.4 Limitations 31

D.5 Future work 32

E Experimental Details **32**

E.1 Pre-training & Post-training 32

E.2 Evaluation benchmarks 34

E.3 ImageNet classification 34

E.4 Grad-CAM 34

E.5 Semantic segmentation 35

E.6 Representation alignment 35

E.7 PIVOT-enhanced vision model evaluation 35

A Related Work

A.1 MLLMs.

Building on the success of LLMs, the development of MLLMs has become a prominent research direction for equipping LLMs with visual understanding (Team et al., 2024a; Achiam et al., 2023; Bai et al., 2023b). The standard paradigm involves connecting a pretrained vision encoder to an LLM via a multimodal projector, creating a strong baseline (Liu et al., 2023a; Li et al., 2023a; Jaegle et al., 2022). Subsequent advancements have been achieved by employing larger components (Li et al., 2024b), training on higher-quality conversational data (Li et al., 2025a; Bai et al., 2025; Han et al., 2025), or introducing new techniques for stronger visual understanding (Kar et al., 2024; Lin et al., 2024; Tong et al., 2024b). The dominant training strategy for these models has been SFT (Touvron et al., 2023a; Brown et al., 2020; Dai et al., 2019), where the model learns to generate a ground-truth response for a given visual input and query. As noted in Cambrian (Tong et al., 2024a), while SFT has been effective, RL is emerging as a promising alternative to potentially surpass the performance ceilings of current methods.

A.2 LLMs with RL.

Following the development of various Transformer-based language models (Raffel et al., 2020; Lewis et al., 2020; Radford et al., 2018; Touvron et al., 2023a; Bai et al., 2023a), trained with objectives such as masked modeling (Devlin et al., 2019) and SFT, a major breakthrough was achieved by aligning LLMs with human preferences through RLHF (Christiano et al., 2017; Ouyang et al., 2022; Touvron et al., 2023b). The foundational method involved using PPO (Schulman et al., 2017) to optimize an SFT model against a reward model trained on preference data. This paradigm has since evolved: DPO (Rafailov et al., 2023) directly instills preference alignment by optimizing on pairwise preferences, and GRPO (Shao et al., 2024) updates the policy using group-wise relative rankings of candidate responses. This line of research, which also includes methods like IPO (Azar et al., 2024), KTO (Ethayarajh et al., 2024), and ORPO (Hong et al., 2024), has consistently demonstrated the power of RL. Whereas prior works, RL's Razor (Shenfeld et al., 2025) and RL-Squeezes (Matsutani et al., 2025), compared RL and SFT in the context of LLM adaptation to new tasks, we conduct a parallel investigation into how these distinct trainings impact MLLMs.

A.3 MLLMs with RL

The MLLM field is increasingly adopting RL to push beyond the limitations of SFT, mirroring the evolution of LLMs. We provide a comprehensive list in Table A. Several studies (Yu et al., 2025; Xiong et al., 2025), including LLaVA-RLHF (Sun et al., 2024) and MPO (Wang et al., 2024b), have reported that applying additional preference alignment to an SFT-trained MLLM can boost its performance. In parallel, other works have proposed DPO extensions for MLLMs: OPA-DPO (Yang et al., 2025c), and HDPO (Fu et al., 2025b). These approaches reweight token-level losses on disagreement tokens between the chosen and rejected responses, or combine SFT with DPO for joint training. Some studies (Zadeh et al., 2025; Xie et al., 2024), such as CHiP (Fu et al., 2025a) and mDPO (Wang et al., 2024a), have shown that incorporating visual preference data reduces perceptual errors in MLLMs. Finally, Chu et al. (2025) and Li et al. (2025b) have indicated that RL is advantageous for adapting MLLMs' inherent knowledge to special environments, like card games, map navigation, or robot action planning. Our work conducts a controlled comparison between SFT and DPO (Section 3.1) and, unlike RL-vs.-SFT studies (Chu et al., 2025; Li et al., 2025b), evaluates on common benchmarks rather than specialized settings.

A.4 Vision-centric pre-trainings

The pretraining of vision models has largely followed two paths: image-only self-supervised learning and image-language supervised learning. The former, encompassing contrastive (He et al., 2020; Chen et al., 2020; Caron et al., 2020; Chen & He, 2021; Caron et al., 2021) learning and masked-image-modeling (Bao et al., 2022; He et al., 2022), has proven effective for creating visual representation models

Abbreviation	Title	Venue	Year	RL
RLHF-V (Yu et al., 2024)	Towards Trustworthy MLLMs via Behavior Alignment from Fine-grained Correctional Human Feedback	CVPR	2024	DPO
RLAIF-V (Yu et al., 2025)	Open-Source AI Feedback Leads to Super GPT-4V Trustworthiness	CVPR	2025	DPO
LLaVA-RLHF (Sun et al., 2024)	Aligning Large Multimodal Models with Factually Augmented RLHF	ACL	2024	PPO
LLaVA-Critic (Xiong et al., 2025)	Learning to Evaluate Multimodal Models	CVPR	2025	DPO
OPA-DPO (Yang et al., 2025c)	Mitigating Hallucinations in Large Vision-Language Models via DPO: On-Policy Data Hold the Key	CVPR	2025	DPO
HDPO (Fu et al., 2025b)	Mitigating Hallucination in Multimodal Large Language Model via Hallucination-targeted Direct Preference Optimization	ACL	2025	DPO
CHiP (Fu et al., 2025a)	Cross-modal Hierarchical Direct Preference Optimization for Multimodal LLMs	ICLR	2025	DPO
mDPO (Wang et al., 2024a)	Conditional Preference Optimization for Multimodal Large Language Models	EMNLP	2024	DPO
LPOI (Zadeh et al., 2025)	Listwise Preference Optimization for Vision Language Models	ACL	2025	DPO
V-DPO (Xie et al., 2024)	Mitigating Hallucination in Large Vision Language Models via Vision-Guided Direct Preference Optimization	EMNLP	2024	DPO
MPO (Wang et al., 2024b)	Enhancing the Reasoning Ability of Multimodal Large Language Models via Mixed Preference Optimization	arXiv	2024	DPO
LongPerceptualThoughts (Liao et al., 2025)	LongPerceptualThoughts: Distilling System-2 Reasoning for System-1 Perception	arXiv	2025	DPO
SimpleVLA-RL (Li et al., 2025b)	SimpleVLA-RL: Scaling VLA Training via Reinforcement Learning	arXiv	2025	GRPO
RL Generalizes (Chu et al., 2025)	SFT Memorizes, RL Generalizes: A Comparative Study of Foundation Model Post-training	ICML	2025	PPO

Table A List of RL-based MLLM works. We provide an overview of methods with their venues, years, and RL optimization strategies, and note that most of the previous studies have adopted DPO (Rafailov et al., 2023) as an RL baseline.

for classic vision tasks like image classification and segmentation. The latter, as in CLIP (Radford et al., 2021), SigLIP (Zhai et al., 2023; Tschannen et al., 2025), and EvaCLIP (Sun et al., 2023), aligns vision and language, enabling strong zero-shot recognition and making these models popular backbones for MLLMs (Li et al., 2025a). Our PIVOT is a CLIP-style alternative for training vision encoders, as both use language-aligned supervision. Applied to existing encoders, PIVOT transforms them into MLLM-ready encoders with $<$1% of the GPUs and data relative to SigLIP2 training.

Recently, Perception Encoder (Bolya et al., 2025) explored improved recipes for building powerful vision encoders through vision-language pre-training. Its language alignment stage follows a strategy similar to the '+ SFT' setting in Table 2. Unlike their focus on SFT-driven representation changes, we investigate how RL training influences vision representations.

B Additional Experiments

B.1 Other RL algorithms vs. SFT

Rationale for Focusing on DPO. In our analysis, we focus on DPO as the primary RL method. This choice reflects practical considerations in MLLM post-training. **DPO** (Rafailov et al., 2023) avoids dependence on a reward model, reducing confounding factors when comparing with SFT. It also operates on a data format similar to SFT, (I_i, q_i, y_i^c, y_i^r), enabling a controlled comparison with the same number of image–query–response pairs, as described in Section 3.1. In contrast, **PPO** (Schulman et al., 2017) requires an external reward model trained on a separate dataset and introduces additional RLHF data, making a fair comparison with SFT difficult. **GRPO** (Shao et al., 2024) depends on verifiable signals such as math or coding problems for LLMs, or object counting and bounding-box annotations for MLLMs. These properties differ from those of typical SFT datasets, hindering the construction of a matched evaluation setup. While these constraints motivated our focus on DPO, we also extend our experiments to PPO,

Code	Task	GRPO data	SFT data	GRPO code	SFT code	Vision encoder
R1-V (2025)	object counting / geometry math	✓	✗	✓	✓	update
EasyR1 (2025)	geometry math	✓	✗	✓	✗	update
SimpleVLA-RL (2025b)	robot action planning	✓	✗	✓	✗	freeze
VLM-R1 (2025)	bounding-box annotation	✓	✓	✓	✓	update

Code	Task	PPO data	SFT data	PPO code	SFT code	Vision encoder
RL4VLM (2024)	card game / robot action planning	✓	✓	✓	✗	freeze
RL Generalize (2025)	card game / navigation	✓	✗	✓	✓	update
LLaVA-RLHF (2024)	conversation	✓	✓	✓	✓	freeze

Table B Overview of GRPO- and PPO-based MLLM GitHub repository. We summarize open-source implementations for RL-based MLLM training, highlighting their main tasks, data and code availability, and encoder update strategies.

Model	Post-train	Avg (All)	General	OCR&Chart	Vision	Knowledge
LLaVA-1.0-7B	SFT	33.1	43.6	26.8	26.7	35.2
LLaVA-1.0-7B	PPO	**34.6**	**44.0**	**30.0**	**28.0**	**36.4**
	Δ	+1.5	+0.4	+3.2	+1.3	+1.2

Table C Evaluation of LLaVA-1.0-7B under PPO vs. SFT post-training. We present results on MLLM benchmarks for MLLMs trained with different objectives (left).

GRPO, and a DPO variant (*i.e.*, MPO (Wang et al., 2024b)) to validate that our findings generalize beyond DPO.

GRPO vs. SFT. The main results of GRPO vs. SFT are presented in Section 5. Here we provide additional details on the experimental setup. We first survey publicly available implementations of GRPO, as summarized in Table B. Among them, we adopt the codebase from VLM-R1, as it provides a *validated* training strategy for proper GRPO implementation. To prevent GPU memory issues during evaluation, we fix the input image resolution to 664×664. For vision-only evaluation, we resize images to 336×336 to extract visual representations and use features prior to the adaptor.

PPO vs. SFT. We next turn to the comparison between PPO and SFT and provide a survey of available codebases, as presented in Table B. Based on these conditions, we choose to adopt the LLaVA-RLHF (Sun et al., 2024) implementation. For PPO, we utilize their publicly released model. For SFT, we post-train a LLaVA-1.0-7B model for one epoch using their SFT data under the original LLaVA framework (Liu et al., 2023a). We note that LLaVA employs the CLIP-L/14-224px encoder, where all input images are automatically resized to 224×224. We present the results in Table C and observe that the PPO-trained MLLM outperforms its SFT counterpart across 16 MLLM benchmarks, with a notable gain on OCR&Chart tasks. We also note that LLaVA-1.0-13B is used as the reward model in this codebase, introducing confounding factors beyond the training objectives alone. Our DPO vs. SFT comparison mitigates this issue by avoiding a reward model and therefore provides a clearer perspective on RL versus SFT, consistent with prior works summarized in Table A.

MPO vs. DPO vs. SFT. Finally, we extend our comparison by including MPO (Wang et al., 2024b) as a variant of DPO. Mixed preference optimization (i.e., MPO) combines the objectives of DPO, SFT, and a binary preference classification loss. We integrate their implementation into our codebase and run the experiments. The Table D (top & middle) reports MLLM and vision-only evaluation results under different MLLM training algorithms. MPO achieves the highest average score in the MLLM evaluation, outperforming SFT, though its gain over DPO remains modest. On vision-only benchmarks, MPO matches DPO, suggesting that its impact on visual representation learning is limited. Moreover, we present additional results in Table D (bottom), following Section 6.1, where visual representations are evaluated within MLLMs. The results demonstrate that DPO and MPO both improve visual representation quality over SFT, with MPO showing slight gains in vision-centric and knowledge tasks.

Overall, our experiments with GRPO, PPO, and MPO demonstrate that RL-based training improves MLLM performance and visual representations beyond SFT, confirming that our findings hold across other RL algorithms. The full results across the 16 benchmarks are provided in Table M and Table N.

Model	Post-train	Avg	General	OCR&Char	Vision	Knowledge
Qwen2.5-1.5B + SigLIP2-L/16	SFT	59.4	68.0	60.9	56.4	52.4
Qwen2.5-1.5B + SigLIP2-L/16	DPO	61.0	70.0	**62.6**	58.4	53.0
Qwen2.5-1.5B + SigLIP2-L/16	MPO	**61.5**	**70.2**	62.2	**59.6**	**54.0**

Model	Post-train	ImageNet	Segmentation
Qwen2.5-1.5B + SigLIP2-L/16	SFT	48.53	30.18
Qwen2.5-1.5B + SigLIP2-L/16	DPO	**50.51**	30.89
Qwen2.5-1.5B + SigLIP2-L/16	MPO	50.18	**31.07**

MLLM = Qwen1.5-1.5B	Avg (All)	General	OCR&Char	Vision	Knowledge
+ Original SigLIP2-So/16	52.4	66.2	46.6	50.6	46.1
+ Stage2-SFT	54.6	66.9	52.2	51.7	47.7
+ Stage2-DPO (i.e., PIVOT)	**55.6**	**68.1**	**53.9**	52.4	48.1
+ Stage2-MPO	**55.6**	67.9	53.8	**52.6**	**48.3**

Table D Evaluation of MLLMs under SFT, DPO, and MPO post-training. We present results on MLLM benchmarks for models trained with different post-training objectives (top). We further evaluate the updated vision encoder on vision-only benchmarks (middle), and finally assess the same encoder when re-integrated and evaluated within MLLMs (bottom).

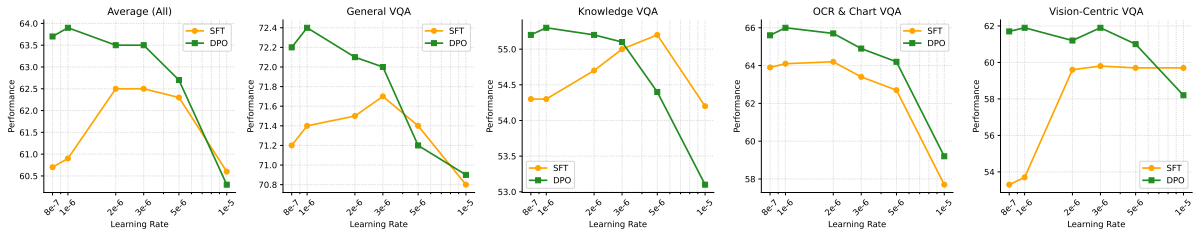


Figure A Training sensitivity in Multimodal LLMs. We conduct an analysis of performance with respect to learning rate under different post-tuning strategies, using Qwen2.5-3B combined with SigLIP2-So/16. The x-axis shows learning rates on a log scale.

B.2 MLLM Training Sensitivity

We examine how variations in the learning rate (LR) affect MLLM performance under different post-training strategies. We conduct experiments with Qwen2.5-3B and SigLIP2-So/16 and show the results in Figure A. Since SFT and DPO rely on fundamentally different loss formulations, their optimal learning rates naturally diverge. In practice, we observe that DPO requires substantially smaller LRs than SFT, partly because DPO accounts for both chosen and rejected responses, effectively doubling the batch size per iteration compared to SFT.

B.3 MLLM performance under new data distributions

Motivation. Previous studies, including RLgeneralize (Chu et al., 2025), SimpleVLA-RL (Li et al., 2025b), and RL-Razor (Shenfeld et al., 2025), have posited that RL is beneficial for adapting to new data distributions, mitigating performance degradation and catastrophic forgetting. Unfortunately, they either focused on specialized environments, such as card gaming and robot action planning, or conducted evaluations confined to the knowledge domain like mathematics. Hence, we examine how our MLLMs behave on more common VQA benchmarks when the *Stage 2* post-training data distribution differs from that of *Stage 1* pre-training.

Experimental setup. The LLaVA-OneVision samples predominantly contain short answers with fewer than 50 words and lack special tokens such as `<think>...</think>` and `<review>...</review>`. In contrast, the MMPR samples occasionally include longer responses and diverse annotation patterns. We exploit this discrepancy by constructing a new *Stage 2* post-training dataset based on MMPR. Specifically, we sample 20K instances from MMPR, where a fraction $r\%$ (0%, 50%, or 80%) consists of samples that either exceed 100 words or contain special tokens. The remaining $100 - r\%$ of the dataset is randomly sampled from the rest of MMPR following our original setup.

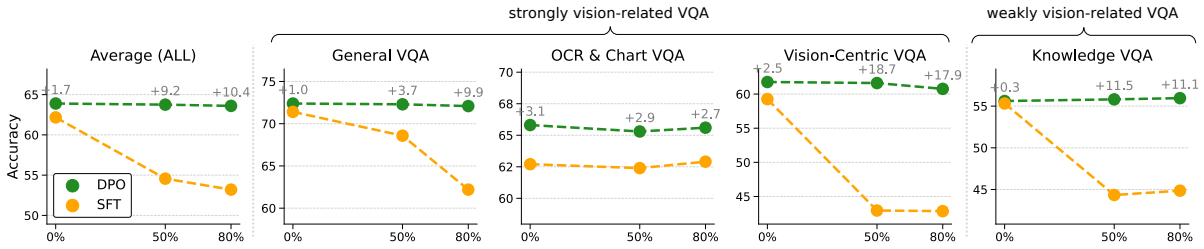


Figure B MLLM training under new data distribution. We post-train (*i.e.*, *Stage 2*) an MLLM (Qwen2.5-3B + SigLIP2-So/16) under varying proportions of samples from a shifted distribution (0%, 50%, 80%). DPO remains stable, while SFT shows substantial declines, particularly on general and vision-centric VQA benchmarks.

LLM backbone	Train	Data	Avg. (All)	General	OCR&Chart	Vision-cent.	Knowledge
Qwen2.5-1.5B	SFT	Origin	59.1	68.3	60.5	54.8	52.8
Qwen2.5-1.5B	DPO	Origin	**61.0**	**69.8**	**63.1**	**57.7**	**53.3**
	Δ		+1.9	+1.5	+2.6	+2.9	+0.5
Qwen2.5-1.5B	SFT	NoThink	59.5	68.9	60.5	56.3	52.4
Qwen2.5-1.5B	DPO	NoThink	**60.8**	**69.3**	**62.3**	**58.3**	**53.2**
	Δ		+1.2	+0.4	+1.7	+2.0	+0.7
Qwen2.5-1.5B	SFT	Under30	59.3	69.0	59.2	56.1	52.8
Qwen2.5-1.5B	DPO	Under30	**60.1**	**69.6**	**60.0**	**57.4**	**53.3**
	Δ		+0.8	+0.6	+0.8	+1.3	+0.5
Qwen2.5-3B	SFT	Origin	62.3	71.4	62.7	59.7	55.2
Qwen2.5-3B	DPO	Origin	**63.9**	**72.4**	**66.0**	**61.9**	**55.3**
	Δ		+1.7	+1.0	+3.3	+2.2	+0.1
Qwen2.5-3B	SFT	NoThink	62.9	71.6	63.8	60.0	**56.2**
Qwen2.5-3B	DPO	NoThink	**63.5**	**71.8**	**64.1**	**62.5**	55.6
	Δ		+0.6	+0.2	+0.3	+2.5	-0.6
Qwen2.5-3B	SFT	Under30	62.5	71.0	64.0	59.4	**55.8**
Qwen2.5-3B	DPO	Under30	**63.0**	**71.4**	**64.1**	**61.6**	55.0
	Δ		+0.5	+0.5	+0.1	+2.2	-0.8

Table E MLLM training with SFT-friendly datasets. We train Qwen2.5-based MLLMs using different data configurations (Origin, NoThink, Under30) and evaluate them on 16 multimodal benchmarks. The vision encoder used in all MLLMs is fixed to SigLIP2-So/16.

Results. The results, shown in Figure B, reveal that DPO maintains robust performance even as the proportion of new-distribution samples increases. In contrast, SFT-trained MLLMs experience a sharp decline: while achieving 62.2%p with 0% of new-distribution samples, their performance drops to 53.2%p when the ratio increases to 80%. The degradation is especially pronounced in vision-centric VQA tasks, where the accuracy gap between DPO and SFT reaches 17.9%p with 80% new-distribution samples. It demonstrates that the trends observed in earlier RL studies (Chu et al., 2025; Li et al., 2025b; Shenfeld et al., 2025) also generalize across the broad set of 16 benchmarks considered in our evaluation.

B.4 MLLM performance under more SFT-friendly data

Motivation. In our main experiments, we use the MPO (Wang et al., 2024b) dataset for post-training. Since this dataset is originally designed for DPO supervision, it may inherently favor DPO. To mitigate this concern and examine whether the relative performance depends on the data characteristics, we additionally construct post-training datasets that are intentionally more SFT-friendly.

Setup. We again sample 20K instances from MPO and apply the following constraints to each pair (I_t, x_t, y_t^c, y_t^r). The 'Under30' setting retains only samples where the chosen response y_t^c contains fewer than 30 words, similar in style to 'clear-answer' data. The 'NoThink' setting removes samples containing special reasoning tokens (e.g., `<think>`, `<review>`) and restricts y_t^c to fewer than 60 words. These filters yield datasets that align more closely with typical SFT supervision, reducing the implicit advantage that DPO may receive from the original MPO distribution. We repeat the SFT–DPO comparison of Section 3.1 using Qwen2.5-1.5B and Qwen2.5-3B as the LLM backbone, paired with SigLIP2-So/16. The results are summarized in Table E.

Model	Avg (All)	HallusionBench (2024)			POPE (2023b)		
		AnswerAcc	FaithAcc	QuestionAcc	precision	recall	f1
MLLM-0.5B-SFT	51.43	33.22	**12.42**	9.23	89.71	79.63	84.37
MLLM-0.5B-DPO	**54.76**	**37.85**	11.84	**15.6**	**93.71**	**82.06**	**87.5**
MLLM-1.5B-SFT	56.31	40.79	21.09	15.6	92.89	**80.98**	86.53
MLLM-1.5B-DPO	**58.97**	**48.79**	**22.83**	**21.09**	**94.53**	79.95	**86.63**

Model	Avg (All)	MS COCO (2015)			DetailCaps-4870 (2024)		
		METEOR	ROUGE-L	BERTScore	METEOR	ROUGE-L	CAPTURE
MLLM-0.5B-SFT	41.03	**28.22**	50.34	67.11	16.77	26.65	57.07
MLLM-0.5B-DPO	**41.47**	27.63	**51.07**	**67.81**	**17.27**	**27.37**	**57.64**
MLLM-1.5B-SFT	40.84	27.61	47.98	66.17	17.25	**27.82**	58.18
MLLM-1.5B-DPO	**42.10**	**28.52**	**50.64**	**68.46**	**18.48**	27.08	**59.44**

Model	Avg (All)	NaturalBench (2024a)			MME_Real. (2025)	VLReward (2025c)
		GroupAcc	ImageAcc	QuestionAcc	Avg	Avg
MLLM-0.5B-SFT	12.65	12.84	42.18	0.3695	22.07	**43.27**
MLLM-0.5B-DPO	**14.27**	**17.84**	**47.61**	**0.4213**	**27.24**	43.02
MLLM-1.5B-SFT	13.75	16.53	44.03	0.4042	27.21	40.55
MLLM-1.5B-DPO	**14.49**	**25.05**	**54.08**	**0.5087**	**28.35**	**42.82**

Table F Comparison of DPO vs. SFT across extended MLLM benchmarks. We present results on hallucination, captioning, and real-world/robustness benchmarks. We use MLLMs in Section 3.

Results. We observe that these SFT-friendly datasets reduce the data-efficiency advantage of DPO. However, its performance does not fall below that of SFT. We hypothesize that the shorter responses decrease the informational gap between chosen and rejected samples, which diminishes DPO's effectiveness. Nevertheless, DPO does not fall behind SFT; its performance remains better even under these SFT-friendly conditions. The full results across the 16 benchmarks are provided in Table O.

B.5 MLLM performance on hallucination, captioning, and robustness benchmarks

Setup. We extend our analysis to a broader set of vision tasks to assess the generality of our findings. As summarized in Table F, we evaluate models on hallucination, captioning, and real-world robustness benchmarks. For hallucination, we include HallusionBench (Guan et al., 2024) and POPE (Li et al., 2023b). For captioning, we use MS COCO (Chen et al., 2015) and DetailCaps-4870 (Dong et al., 2024), which emphasize descriptive completeness. For robustness, we incorporate NaturalBench (Li et al., 2024a), MME-RealWorld (Zhang et al., 2025), and VL-RewardBench (Li et al., 2025c). Specifically, NaturalBench assesses visual grounding robustness by mitigating reliance on language priors, MME-RealWorld evaluates practical utility in complex real-world environments, and VL-RewardBench measures alignment with human preferences across diverse multimodal domains.

Results. Across all benchmarks, DPO consistently outperforms SFT. As discussed in Section 4, we attribute these gains to the contrastive nature of DPO, which provides fine-grained gradient signals to the vision encoder and strengthens the model's visual understanding. These enhanced visual representations translate into improved performance on captioning, hallucination mitigation, and real-world robustness evaluations.

B.6 MLLM performance on text-only benchmarks

To examine whether multimodal post-training affects language-only abilities, we evaluate the resulting MLLMs on several text-only benchmarks, as summarized in Table G. Our evaluation includes HellaSwag (Zellers et al., 2019), MMLU (Hendrycks et al., 2021), and GSM8K (Cobbe et al., 2021), which are widely used for assessing LLM general language understanding. Results show that DPO-trained models achieve superior performance on MMLU compared to SFT. For HellaSwag and GSM8K, performance remains comparable, aligning with observations in Knowledge VQA. We speculate that this is due to the data distribution of MPO (Wang et al., 2024b), which is used for multimodal training. MPO data includes general, science, and document VQA data, which overlaps with the target of MMLU. However, MPO's

Model	MMLU (2021)					HellaSwag (2019)	GSM8K (2021)
	Overall	Humanities	Other	SocialSci	STEM	Acc	Acc
MLLM-0.5B-SFT	30.7	31.2	33.9	31.7	25.8	**45.8**	33.4
MLLM-0.5B-DPO	**38.1**	**37.3**	**43.9**	**40.3**	**31.2**	45.3	**34.7**
Δ	+7.4	+6.1	+10.0	+8.6	+5.5	-0.5	+1.3
MLLM-1.5B-SFT	34.7	32.8	39.0	38.0	29.8	55.4	**57.7**
MLLM-1.5B-DPO	**46.8**	**42.7**	**51.6**	**54.5**	**40.5**	**56.9**	57.3
Δ	+12.1	+9.9	+12.5	+16.5	+10.7	+1.6	-0.4

Table G Evaluation on text-only benchmarks. We report MMLU, HellaSwag, and GSM8K performance of SFT vs. DPO trained MLLMs across two model scales.

Evolving vision encoder				MLLM combining the vision encoder with Qwen2.5						
Vision encoder	# Params	PIVOT-proj.	LLM	Add. layer	Total layer	Avg. (All)	General.	OCR&Chart.	Vision-Cen.	Knowledge.
SigLIP2-So/16$_{+\text{PIVOT}}$	400M	0	Qwen2.5-0.5B	2	2	42.9	56.3	39.1	37.9	38.3
SigLIP2-So/16$_{+\text{PIVOT}}$	400M	2	Qwen2.5-0.5B	2	4	44.3	56.5	39.8	41.4	39.4
SigLIP2-So/16$_{+\text{PIVOT}}$	400M	1	Qwen2.5-0.5B	1	2	**45.2**	**57.8**	**39.5**	**43.4**	**40.3**
SigLIP2-So/16$_{+\text{PIVOT}}$	400M	0	Qwen2.5-1.5B	2	2	52.4	66.2	46.1	46.6	50.6
SigLIP2-So/16$_{+\text{PIVOT}}$	400M	2	Qwen2.5-1.5B	2	4	54.3	66.4	48.2	49.7	52.9
SigLIP2-So/16$_{+\text{PIVOT}}$	400M	1	Qwen2.5-1.5B	1	2	**54.6**	**66.7**	**47.1**	**50.8**	**54.0**

Table H Ablation on reusing the PIVOT-trained projector. 'PIVOT-projector 0, 1, 2' denote configurations that reuse none, only the first layer, or two layers of the frozen PIVOT-trained projector, respectively. Additional trainable layers during the evaluation setup of Figure 11 are appended before the LLM to match dimensionality. Among these, the 1+1 setup—reusing the first frozen layer with one new layer—achieves the best downstream MLLM performance.

math data is highly focused on geometry that GSM8K doesn't cover. Also, MPO doesn't have data related to HellaSwag tasks. Thus, we conjecture that the data overlap causes different results between MMLU and others. Still, an in-depth study is needed, which we consider future work.

B.7 PIVOT ablation study

Beyond the results in Section 6, we perform further experiments to gain deeper insights into PIVOT.

PIVOT-enhanced projector. (**setup**) There are two components responsible for visual representation in an MLLM: the vision encoder and the projector. In this section, we extend the analysis to the projector, investigating whether reusing the PIVOT-tuned projector benefits the model under the same setting. The PIVOT-tuned projector obtained after *Stage 2* follows our standard MLLM architecture, consisting of a two-layer MLP. During downstream MLLM training in Section 6.1, we vary which part of this projector is reused, and denote the configurations as 'PIVOT-tuned 0, 1, and 2,' corresponding to using none, only the first linear layer, or the entire two-layer MLP, respectively.

The PIVOT-tuned vision encoder and projector must be connected to a new LLM for downstream evaluation of Figure 11. To enable this, we introduce a new set of MLP layers, referred to as the additional projector. We vary the number of layers in this module, and define the total number of multimodal linear layers as the sum of those from the PIVOT-tuned projector and the additional projector. For example, "PIVOT projector 2, Add. layer 2" indicates that the two frozen layers from the PIVOT-tuned projector are reused, while two additional randomly initialized layers are appended in the additional projector, resulting in a total of four layers. (**results**) We observe that using the first linear layer from the PIVOT-tuned projector together with one additional layer (i.e., two layers in total) yields the best downstream MLLM performance. Contrary to the expectation that increasing the depth (e.g., 2+2 layers) would leverage more parameters and improve results, this configuration instead leads to inferior performance. Based on this finding, we adopt the 1+1 setting for all subsequent experiments in Section 6.

Training with more data. In Section 6.1, our PIVOT-enhanced vision encoder is paired with a new LLM and finetuned on the Cambrian-737K dataset. We examine whether the same trend holds with larger-scale data during evaluation in Figure 11 by using the LLaVA-OV-3M dataset. The results are reported in Table I. Our findings confirm that the advantage of PIVOT persists even with more data. For example, when combined with Qwen2.5-1.5B, the PIVOT-enhanced SigLIP2-So/16 achieves an average gain of +2.3%p over the base SigLIP2-So/16 encoder, demonstrating that the benefits of PIVOT are robust to

Evolving vision encoder		MLLM combining the vision encoder with Qwen2.5						
Vision encoder	# Params	LLM	Data	Avg. (All)	General.	OCR&Chart.	Vision-Cen.	Knowledge.
SigLIP2-So/16	400M	Qwen2.5-1.5B	Cambrian-737K	52.4	66.2	46.6	50.6	46.1
+PIVOT	400M	Qwen2.5-1.5B	Cambrian-737K	**55.6**	**68.1**	**53.9**	**52.4**	**48.1**
Δ				+3.2	+1.9	+7.3	+1.8	+2.0
SigLIP2-So/16	400M	Qwen2.5-1.5B	LLaVA-OV-3M	56.9	67.9	56.4	51.3	52.0
+PIVOT	400M	Qwen2.5-1.5B	LLaVA-OV-3M	**59.2**	**68.9**	**59.8**	**54.6**	**53.5**
Δ				+2.3	+1.0	+3.4	+3.3	+1.5
SigLIP2-So/16	400M	Qwen2.5-0.5B	LLaVA-OV-3M	49.0	58.8	47.2	45.2	44.6
+PIVOT	400M	Qwen2.5-0.5B	LLaVA-OV-3M	**50.6**	**59.9**	**51.0**	**46.5**	**45.1**
Δ				+1.6	+1.1	+3.8	+1.3	+0.5

Table I Effect of larger Stage 3 data on PIVOT performance. Comparison between basic and PIVOT-enhanced SigLIP2-So/16 encoders paired with Qwen2.5, trained on either Cambrian-737K (Tong et al., 2024a) or LLaVA-OV-3M (Li et al., 2025a). PIVOT consistently improves MLLM performance, and its advantage remains robust even with larger-scale training data.

Evolving vision encoder		MLLM combining the vision encoder with Qwen2.5						
Vision encoder	# Params	LLM	Full train?	Avg. (All)	General.	OCR&Chart.	Vision-Cen.	Knowledge.
SigLIP2-So/16	400M	Qwen2.5-0.5B	✓	45.1	57.1	44.6	39.6	39.2
+ PIVOT	400M	Qwen2.5-0.5B	✓	**46.0**	**58.2**	**45.0**	**41.5**	**39.4**
Δ				+0.9	+1.1	+0.4	+1.9	+0.2
SigLIP2-So/16	400M	Qwen2.5-1.5B	✗	52.4	66.2	46.6	50.6	46.1
SigLIP2-So/16	400M	Qwen2.5-1.5B	✓	54.5	67.1	51.1	53.1	46.9
+ PIVOT	400M	Qwen2.5-1.5B	✓	**55.2**	**67.5**	**52.1**	**54.1**	**47.2**
Δ				+0.7	+0.4	+1.0	+1.0	+0.3

Table J Effect of full-parameter training. Although updating all model parameters inevitably alters the intrinsic representations of the vision encoder, we aim to understand its overall effect. MLLMs incorporating PIVOT-enhanced encoders exhibit clear and consistent gains over their baseline counterparts, highlighting the robustness of PIVOT beyond the controlled evaluation protocol.

data scale.

Training all parameters. We adopt the same evaluation protocol of Cambrian (Tong et al., 2024a), DINO-MLLM (Fan et al., 2025), and MLLM-data (Han et al., 2025) in order to directly assess how useful the visual representations of a vision encoder itself are for an MLLM. As noted by Cambrian, it allows us to study visual representations efficiently. Obviously, training all parameters of the model during the evaluation setup of Figure 11 alters the intrinsic representations of the encoder. Nevertheless, we were interested in understanding how the MLLM performance changes when all parameters—including the vision encoder, LLM, and projector—are updated during *Stage 3*. The results, reported in Table J, show that MLLMs built upon PIVOT-enhanced encoders consistently outperform their counterparts.

B.8 PIVOT performance comparison with existing MLLMs

To more comprehensively evaluate PIVOT-based MLLMs in Section 6, we compare its performance against existing multimodal models. Our evaluation covers BLIP-2 (Li et al., 2023a), LLaVA-1.5 (Liu et al., 2024a), LLaVA-Next (Li et al., 2024b), LLaVA-OneVision (Li et al., 2025a), and SPHINX (Lin et al., 2024). The results in Table K show that our MLLM with PIVOT achieves strong performance. Moreover, PIVOT (1.5B) outperforms other MLLMs built on language models under 2B parameters and even exceeds larger models such as LLaVA-1.5B, BLIP-2, and SPHINX. Full results across the 16 benchmarks are provided in Table P.

C Extended Results from the Main Paper

C.1 MLLM training data scaling

In Figure 4, we analyze the effect of post-training data scale on MLLM performance, focusing on the average scores across all benchmarks. To complement this, we provide the results for each specific domain in Figure C. The results consistently show that the DPO-tuned MLLM outperforms its SFT

Model	LLM size	Avg. (All)	General	OCR&Chart	Vision-Cent.	Knowledge
BLIP-2 (2023a)	7B	43.7	48.5	52.8	31.0	42.5
SPHINX (2024)	7B	48.7	65.6	33.2	52.5	41.4
LLaVA-Next-Vincina (2024b)	7B	50.6	68.3	38.0	52.8	43.9
LLaVA-Next-LLaMA-3 (2024b)	8B	60.4	**71.3**	**64.3**	57.5	49.0
LLaVA-Next-Qwen2 (2024b)	7B	**62.0**	70.5	63.3	**62.3**	**53.3**
SPHINX-Tiny (2024)	1.1B	37.5	54.2	19.3	43.6	33.2
LLaVA-OneVision (2025a)	0.5B	50.0	60.4	**57.0**	42.7	39.4
Ours (SigLIP1-So/16)+PIVOT	1.5B	53.2	67.7	46.8	51.7	46.6
Ours (SigLIP2-So/16)+PIVOT	1.5B	**55.6**	**68.1**	53.9	**52.4**	**48.1**

Table K Comparison between PIVOT-based MLLMs and existing models. We evaluate several 7B–8B large models and

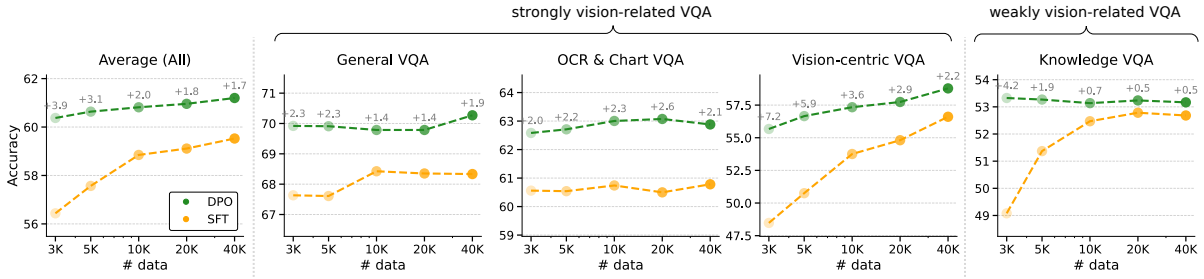


Figure C Scaling the amount of post-training data for MLLM. We vary the size of training data for an MLLM built with Qwen2.5-1.5B and SigLIP2-So/16 and measure its performance.

counterpart as the amount of training data increases. For Knowledge VQA, interestingly, we observe that the performance gap between the two models diminishes from +4.2 to +0.7 as the data size increases from 3K to 10K samples.

Moreover, we examine whether the superiority of DPO persists when training MLLMs with larger datasets. Although SFT exhibits a strong positive slope from 3K to 40K in Figure 4, Table L demonstrates that this trend does not hold as the data scale continues to increase. With more data, the slope becomes negative and SFT fails to catch up with DPO. In our experimental setup, all hyperparameters are fixed except for the dataset size. It is worth noting that selecting hyperparameters suited to the longer training regime can mitigate the performance degradation observed with large amounts of data; for example, adjusting the learning rate or weight decay may help.

C.2 Performance of MLLMs on all 16 benchmarks

Full results on MLLM performance are reported in Table Q, Table R, and Table S. Within our controlled setup, DPO-trained MLLMs consistently surpass their SFT-trained models across different scales of data, vision encoders, and language models. The advantage is evident on 'strongly vision-related tasks' and appears more modest on 'weakly vision-related tasks', corresponding to the experiments in Section 3

C.3 ImageNet classification with a vision encoder

We present additional experimental results for ImageNet classification in Figure D. For this analysis, we conduct a linear-probe evaluation using features obtained from the MLLM's vision encoder. This setup differs from the main paper's experiment in Figure 6, which utilizes visual embeddings that have passed through both the vision encoder and the projector. The results reinforce our primary findings: DPO consistently enhances visual representations more effectively than SFT, and the vision encoder's performance improves as the size of the LLM it is trained with increases.

DPO Data Size	Avg. (All)	General	OCR&Chart	Vision-Cent.	Knowledge
20K	61.0	70.0	62.6	58.4	53.0
40K	61.2	**70.3**	62.6	**58.8**	53.2
60K	**61.4**	69.6	**64.0**	57.9	**54.1**
80K	60.9	69.7	62.4	58.7	53.0
100K	59.8	69.3	60.8	55.9	53.3
150K	54.7	65.0	50.1	52.4	51.3

SFT Data Size	Avg. (All)	General	OCR&Chart	Vision-Cent.	Knowledge
20K	59.4	68.0	60.9	56.4	52.4
40K	59.5	68.0	60.8	**56.6**	52.7
60K	**59.6**	**68.4**	**61.1**	55.0	**53.9**
80K	59.1	67.8	59.5	55.8	53.1
100K	58.1	67.2	57.7	54.5	53.1
150K	55.7	66.4	52.3	52.5	51.8

Table L Scaling the amount of post-training data for MLLM. We provide supplementary quantitative results corresponding to Figure C.

		General				OCR & Chart				Vision-Centric				Knowledge			
Model	Train	MME^P	MMB	$SEED^I$	GQA	ChartQA	OCRBench	TextVQA	DocVQA	MMVP	RealWorldQA	$CV\text{-}Bench^{2D}$	$CV\text{-}Bench^{3D}$	SQA^I	$MMMU^V$	$MathVista^M$	AI2D
QwenVL-2.5-3B	SFT	1536.7	73.4	71.2	56.0	62.9	64.0	62.5	86.7	44.0	50.1	67.4	70.4	78.0	44.0	21.7	76.5
QwenVL-2.5-3B	**GRPO**	1575.8	77.1	73.3	59.2	70.4	67.7	66.8	88.3	43.0	58.2	70.6	74.0	79.3	46.4	22.6	78.5
LLaVA-1.0-7B	SFT	1201.1	39.3	42.5	32.5	7.1	21.6	34.8	43.8	10.9	31.3	25.0	39.5	64.8	27.9	3.1	45.0
LLaVA-1.0-7B	**PPO**	1230.6	39.5	43.0	32.2	15.7	24.8	34.8	44.8	15.2	33.5	25.0	38.4	64.7	28.1	4.4	48.4
Qwen2.5-1.5B + SigLIP2-L/16	SFT	1420.5	70.9	71.7	58.5	62.4	58.9	64.5	58.0	44.6	58.2	63.6	59.3	86.0	40.2	12.1	71.1
Qwen2.5-1.5B + SigLIP2-L/16	DPO	1485.1	72.4	72.9	60.3	65.2	61.4	64.1	59.5	51.3	58.8	63.2	60.2	86.2	40.8	14.0	71.1
Qwen2.5-1.5B + SigLIP2-L/16	**MPO**	1496.7	72.3	72.4	61.1	65.2	60.4	64.1	59.1	53.3	59.6	63.3	62.2	87.0	41.8	15.3	72.0

Table M Full results of other RL vs. SFT. The table presents the 16-benchmark performance for MLLMs post-trained with SFT, GRPO, PPO, and MPO.

C.4 Gradient visualization of a vision encoder

We provide additional Grad-CAM results in Figure E, where we visualize the gradients on the visual features induced by the SFT and DPO losses. The results show that MLLM post-training yields larger gradients on question-relevant image regions, with DPO providing more concentrated signals than the diffuse gradients from SFT.

Furthermore, the bottom two examples in Figure E correspond to a global query (like "Describe the photo in detail."). For this type of query, both DPO and SFT generate similarly distributed gradients across the entire image, a different outcome from the localized queries. As will be further discussed in Section D.5, this supports our hypothesis that the nature of the post-training data can determine how DPO enhances visual representations.

C.5 Segmentation probing with a vision encoder

We provide additional qualitative results for segmentation probing in Figure F. For this experiment, a CLIP-L/14 336px vision encoder is post-trained in an MLLM with either SFT or DPO, using a Qwen2.5-3B as the base LLM. The qualitative results indicate that the DPO-trained vision encoder yields segmentation maps more consistent with the ground truth.

MLLM = Qwen1.5-1.5B	General				OCR & Chart				Vision-Centric				Knowledge			
	MME^{P}	MMB	$SEED^{I}$	GQA	ChartQA	OCRBench	TextVQA	DocVQA	MMVP	RealWorldQA	$CV\text{-}Bench^{2D}$	$CV\text{-}Bench^{3D}$	SQA^{I}	$MMMU^{V}$	$MathVista^{M}$	AI2D
+ Original SigLIP2-So/16	1403.0	65.8	68.9	59.8	43.5	39.3	54.0	49.5	36.0	55.4	58.2	52.8	72.9	38.2	8.8	64.4
+ Stage2-SFT	1417.0	65.9	70.4	60.5	54.4	45.6	57.8	51.0	36.3	54.8	60.0	55.8	73.3	40.9	11.6	64.9
+ Stage2-DPO (i.e., PIVOT)	1427.5	67.8	71.8	61.4	57.0	48.3	58.5	51.7	38.3	56.2	59.1	56.2	73.9	41.5	12.3	64.7
+ Stage2-MPO	1438.9	68.3	71.0	60.3	56.6	49.1	59.0	50.5	39.0	55.2	60.5	55.6	72.3	41.4	13.8	65.5

Table N Full results under PIVOT evaluation. We first post-train MLLMs using different algorithms and extract their vision encoders, which are evaluated following Section 6.1. Here, we present the full evaluation results across 16 MLLM benchmarks.

LLM backbone	Train	Data	General				Knowledge				Vision-Centric				OCR & Chart			
			MME^{P}	MMB	$SEED^{I}$	GQA	ChartQA	OCRBench	TextVQA	DocVQA	MMVP	RealWorldQA	$CV\text{-}Bench^{2D}$	$CV\text{-}Bench^{3D}$	SQA^{I}	$MMMU^{V}$	$MathVista^{M}$	AI2D
Qwen2.5-1.5B	DPO	Origin	1478.7	71.9	72.5	60.9	65.4	62.7	64.7	59.5	50.0	57.4	63.6	59.9	86.7	40.1	14.7	71.5
Qwen2.5-1.5B	SFT	Origin	1442.1	70.6	71.9	58.7	62.1	58.8	63.4	57.7	44.0	56.0	63.1	56.1	86.6	41.0	12.6	70.9
Qwen2.5-1.5B	DPO	NoThink	1441.4	72.3	72.7	60.3	64.6	61.8	63.8	58.9	47.3	59.0	64.9	62.0	86.1	40.1	15.1	71.3
Qwen2.5-1.5B	SFT	NoThink	1471.6	71.4	71.7	59.1	62.6	58.8	64.8	56.0	46.7	58.8	63.3	56.3	85.5	41.0	13.1	70.1
Qwen2.5-1.5B	DPO	Under30	1469.8	72.2	72.3	60.3	59.8	61.7	62.7	55.8	47.3	57.9	63.1	61.4	86.2	40.8	15.1	71.0
Qwen2.5-1.5B	SFT	Under30	1486.6	70.3	71.8	59.6	59.7	57.8	64.2	55.1	45.3	57.4	62.9	59.0	85.9	40.0	15.9	69.2
Qwen2.5-3B	DPO	Origin	1553.1	76.2	74.4	61.5	67.6	62.2	64.4	69.9	52.0	59.0	67.2	69.3	87.0	42.6	15.7	75.9
Qwen2.5-3B	SFT	Origin	1550.0	75.2	73.7	59.3	58.5	60.1	65.1	67.1	47.5	59.0	66.3	65.8	86.8	42.3	15.9	75.9
Qwen2.5-3B	DPO	NoThink	1511.1	76.6	73.4	61.7	64.9	61.2	64.5	65.8	52.7	60.0	67.3	70.0	88.7	43.6	14.4	75.7
Qwen2.5-3B	SFT	NoThink	1537.8	75.9	74.1	59.6	64.6	60.4	66.1	64.1	49.3	57.8	66.1	66.7	87.4	43.1	18.7	75.6
Qwen2.5-3B	DPO	Under30	1480.2	76.1	74.1	61.4	65.2	62.5	62.9	65.9	53.3	57.8	66.3	68.9	87.6	42.4	15.1	75.0
Qwen2.5-3B	SFT	Under30	1509.2	75.2	73.7	59.5	65.7	59.4	65.8	65.1	50.0	57.1	65.4	65.2	88.3	43.1	17.1	74.7

Table O Full results under SFT-friendly datasets. We provide full evaluation results on 16 MLLM benchmarks.

D Discussions

D.1 Understanding SFT and DPO

We elaborate on the post-training techniques discussed in Section 3.1. SFT is a standard approach for equipping LLMs with instruction-following abilities (Radford et al., 2018; Touvron et al., 2023a). In our work, this involves training the MLLM π_θ using a maximum likelihood objective on the post-training dataset X_{PT}. Specifically, for each given image I_i and query q_i, the model is optimized to maximize the probability of generating the chosen response y_i^c, as formulated in Equation (1). In contrast, DPO (Rafailov et al., 2023) is a prominent RL method that directly aligns the model with human preferences without requiring an explicit reward model. DPO leverages the full preference pair, including both the chosen response y_i^c and the rejected response y_i^r. Its objective, also formulated in Equation (1), is to increase the likelihood of the chosen response while simultaneously decreasing that of the rejected one, relative to a reference policy π_{ref}, which is typically the initial model before preference alignment.

D.2 Low performance gap on Knowledge VQA

As we observe in Section 3, DPO shows a clear advantage over SFT on strongly vision-related tasks, but this performance gap diminishes for Knowledge VQA. This suggests that for knowledge-intensive tasks, leveraging the rejected responses y_i^r provides a less significant benefit compared to the standard SFT

Model	LLM size	General				OCR & Chart				Vision-Centric				Knowledge			
		MME^P	MMB	$SEED^I$	GQA	ChartQA	OCRBench	TextVQA	DocVQA	MMVP	RealWorldQA	$CV\text{-}Bench^{2D}$	$CV\text{-}Bench^{3D}$	SQA^I	$MMMU^V$	$MathVista^M$	AI2D
BLIP-2	7B	1333.7	52.4	17.6	57.3	58.8	43.7	60.1	48.5	23.3	42.4	26.9	31.5	83.0	26.8	11.3	48.8
SPHINX	7B	1515.8	57.6	68.0	61.1	37.8	29.8	38.3	26.8	38.7	48.5	61.3	61.7	68.6	31.6	9.8	55.6
LLaVA-Next-Vincina	7B	1504.2	66.3	68.3	63.2	18.5	33.6	61.0	38.9	30.7	55.3	62.2	62.9	72.3	36.1	7.9	59.2
LLaVA-Next-LLaMA-3	8B	1526.0	71.0	72.6	65.3	69.2	58.1	64.7	65.1	40.0	60.1	62.1	67.7	72.9	39.6	11.8	71.6
LLaVA-Next-Qwen2	7B	1453.3	72.2	73.6	63.6	67.1	54.2	63.6	68.2	49.3	60.0	64.4	75.7	73.5	36.1	30.0	73.7
SPHINX-Tiny	1.1B	1223.8	47.1	57.7	50.8	10.9	18.8	27.0	20.6	14.0	47.6	57.2	55.6	63.0	27.1	1.7	41.1
LLaVA-OneVision	0.5B	1274.9	54.9	63.3	59.5	60.9	60.4	50.9	55.8	18.7	54.1	43.8	54.3	67.5	31.0	4.8	54.3
Ours (SigLIP1-So/16)+PIVOT	1.5B	1446.7	68.7	70.0	59.8	73.8	38.2	9.2	65.2	46.6	36.6	54.7	49.4	36.0	55.8	57.3	57.5
Ours (SigLIP2-So/16)+PIVOT	1.5B	1427.5	67.8	71.8	61.4	57.0	48.3	58.5	51.7	38.3	56.2	59.1	56.2	73.9	41.5	12.3	64.7

Table P Full results of PIVOT-based MLLMs and vs. other MLLMs. The table presents the 16-benchmark performance for diverse MLLMs.

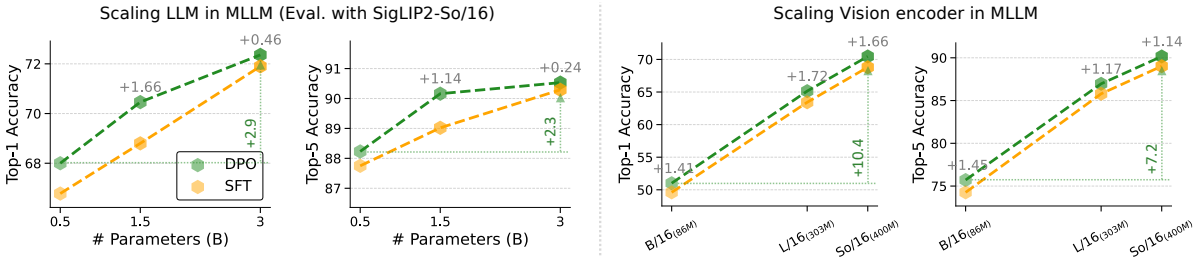


Figure D ImageNet classification. We train MLLMs with different post-training strategies while scaling either the vision encoder (with a fixed Qwen2.5-1.5B) or the LLM (with a fixed SigLIP2-So/16). We utilize features extracted from the MLLM's vision encoder (*i.e.*, SigLIP2-So/16). Note that the features used in Figure 6 are the outputs of the vision encoder and multimodal projector, which are directly used as the LLM's visual embeddings.

approach. We hypothesize that for problems in domains like science and math, the chosen responses y_i^c may already contain sufficient factual knowledge, making the comparative signal from y_i^r less critical. The interplay between preference data characteristics and task domains is a valuable direction for future research.

D.3 Positioning our work within RL-based MLLM research

Prior work has reported performance gains when RL is applied to an MLLM pretrained with SFT (Yu et al., 2024; Wang et al., 2024a; Liao et al., 2025; Fu et al., 2025a). MPO (Wang et al., 2024b) illustrated this by applying DPO to an SFT-trained InternVL model, and RLAIF-V (Yu et al., 2025) similarly compared SFT-trained LLaVA with its DPO-trained variant. Despite this evidence of RL's effectiveness, SFT has remained the dominant training strategy in recent MLLM development (Tong et al., 2024a; Han et al., 2025; Fan et al., 2025). Our study aims to strengthen the RL-based MLLM literature by demonstrating the effectiveness of RL in the post-training stage and motivating its wider adoption in future research. To this end, we design a more fair setup to clearly demonstrate the effect of RL. Rather than comparing a model trained only with SFT to a model trained with SFT followed by DPO, we compare a model trained with SFT in *Stage 1* and DPO in *Stage 2* to a model trained with SFT in both stages. Even under this comparison, we find that DPO remains advantageous, and we hope this result encourages further attention to RL-based approaches in MLLM research.

D.4 Limitations

Despite our efforts in Section 3.1 to design the experimental setup as fairly as possible, our analysis still has limitations. From a data-scale perspective, each DPO update uses (I_t, x_t, y_t^c, y_t^r), whereas SFT relies

Model	Train	Average	General				Knowledge				Vision-Centric				OCR & Chart			
			MME^{P}	MMB	$SEED^{I}$	GQA	SQA^{I}	$MMMU^{V}$	$MathVista^{M}$	AI2D	MMVP	RealWorldQA	$CV\text{-}Bench^{2D}$	$CV\text{-}Bench^{3D}$	ChartQA	OCRBench	TextVQA	DocVQA
Qwen2.5-3B+SigLIP2-B/16	DPO	59.7	1438.4	72.4	72.7	60.1	83.7	44.3	15.7	73.3	45.3	56.9	64.5	65.5	60.5	49.3	59.2	59.3
Qwen2.5-3B+SigLIP2-B/16	SFT	58.3	1509.4	72.2	71.8	57.1	83.6	42.8	15.9	73.5	42.7	55.3	63.7	60.0	57.2	47.0	57.1	57.2
Qwen2.5-3B+SigLIP2-L/16	DPO	62.6	1498.1	75.8	73.6	61.3	85.6	42.3	15.8	74.8	48.7	58.0	66.7	69.3	65.4	58.8	64.2	66.8
Qwen2.5-3B+SigLIP2-L/16	SFT	60.8	1547.8	74.5	73.0	58.3	85.5	42.0	15.5	74.5	43.3	57.6	66.7	65.3	55.1	56.8	62.4	64.1
Qwen2.5-3B+SigLIP2-So/16	DPO	63.9	1553.1	76.2	74.4	61.5	87.0	42.6	15.7	75.9	52.0	59.0	67.2	69.3	67.6	62.2	64.4	69.9
Qwen2.5-3B+SigLIP2-So/16	SFT	62.3	1550.0	75.2	73.7	59.3	86.8	42.3	15.9	75.9	47.5	59.0	66.3	65.8	58.5	60.1	65.1	67.1
Qwen2.5-3B+SigLIP2-g/16	DPO	64.8	1548.6	77.6	75.0	62.5	87.9	43.1	17.2	75.4	52.0	59.1	68.8	70.2	66.0	65.2	67.0	72.3
Qwen2.5-3B+SigLIP2-g/16	SFT	62.9	1558.0	75.7	74.4	60.4	86.9	43.8	17.3	75.3	48.0	59.9	67.5	65.1	57.6	63.8	65.6	67.0

Table Q Scaling the vision encoder in MLLMs. We analyze the impact of the vision encoder sizes, ranging from 86M (SigLIP-B/16) to 1B (SigLIP-g/16) parameters, in Qwen2.5-3B combined with SigLIP2.

only on (I_t, x_t, y_t^c), so the amount of supervision per iteration is not perfectly matched. From a data-type perspective, our comparison relies on preference pairs sourced from the MPO dataset, which may be more favorable to DPO than to SFT. To mitigate these concerns, we make several efforts. Figure 4 shows that even when DPO is limited to fewer samples, it performs strongly, indicating a data-efficiency benefit rather than a data-volume one. In addition, analyses in Section B.3 and Section B.4 examine the impact of different data types and reveal that DPO retains its advantage across these variations. Despite these efforts, further investigation is necessary. A more balanced comparison may require extending SFT to also incorporate negative responses, and it would be valuable to determine whether certain data distributions preferentially benefit SFT or DPO and to identify the properties that underlie such differences.

D.5 Future work

Beyond the broader impact discussed in Section 7, our study opens several additional avenues for research. While our work primarily utilizes the LLaVA Li et al. (2025a) framework with a Qwen2.5 Yang et al. (2025a) backbone, a natural extension is to investigate if our findings generalize to other MLLM architectures, such as InternVL Chen et al. (2024) and Qwen-VL Bai et al. (2023a), or when using different LLM backbones like LLaMA Dubey et al. (2024) and Gemma Team et al. (2024b). Another promising direction involves exploring whether novel dataset formats could be designed to better leverage DPO for learning stronger visual representations. We have **a particular interest** in this direction and plan to actively pursue it as part of our future work.

E Experimental Details

E.1 Pre-training & Post-training

We describe in detail the training strategies of the models used in Section 3. We build our models using the LLaVA-OneVision source code[5]. Our experiments utilize four scales of the SigLIP2 vision encoder (`google/SigLIP2-B/16-patch16-384`, `google/SigLIP2-L/16-patch16-384`, `google/siglip2-So/16-patch16-384`, `google/SigLIP2-g/16-opt-patch16-384`) and four versions of the Qwen2.5-Instruct LLM (`Qwen/Qwen2.5-0.5B-Instruct`, `Qwen/Qwen2.5-1.5B-Instruct`, `Qwen/Qwen2.5-3B-Instruct`, `Qwen/Qwen2.5-7B-Instruct`), which are connected by a 2-layer MLP projector following the default implementation.

For the training data, we use the BLIP_LAION_CC_SBU_558k dataset[6] for projector-only pretraining and the LLaVA-OneVision-Data-Single 3.2M dataset[7] for Stage 1 pretraining. For Stage 2 post-training,

[5] https://github.com/LLaVA-VL/LLaVA-NeXT
[6] https://huggingface.co/datasets/liuhaotian/LLaVA-Pretrain/blob/main/blip_laion_cc_sbu_558k.json
[7] https://huggingface.co/datasets/lmms-lab/LLaVA-OneVision-Data

			General				OCR & Chart				Vision-Centric				Knowledge			
Model	Train	Average	MME^{P}	MMB	$SEED^{I}$	GQA	ChartQA	OCRBench	TextVQA	DocVQA	MMVP	RealWorldQA	CV-Bench^{2D}	CV-Bench^{3D}	SQA^{I}	$MMMU^{V}$	$MathVista^{M}$	AI2D
Qwen2.5-0.5B+SigLIP2-So/16	DPO	51.5	1167.7	58.1	65.7	55.9	76.2	34.1	10.8	59.7	28.0	52.5	52.3	56.5	59.1	56.2	54.8	46.1
Qwen2.5-0.5B+SigLIP2-So/16	SFT	49.5	1170.9	55.2	63.1	55.2	75.1	33.7	10.2	59.1	25.3	50.5	45.3	49.5	57.1	54.3	54.5	45.3
Qwen2.5-1.5B+SigLIP2-So/16	DPO	61.0	1478.7	71.9	72.5	60.9	86.7	40.1	14.7	71.5	50.0	57.4	63.6	59.9	65.4	62.7	64.7	59.5
Qwen2.5-1.5B+SigLIP2-So/16	SFT	59.1	1442.1	70.6	71.9	58.7	86.6	41.0	12.6	70.9	44.0	56.0	63.1	56.1	62.1	58.8	63.4	57.7
Qwen2.5-3B+SigLIP2-So/16	DPO	63.9	1553.1	76.2	74.4	61.5	87.0	42.6	15.7	75.9	52.0	59.0	67.2	69.3	67.6	62.2	64.4	69.9
Qwen2.5-3B+SigLIP2-So/16	SFT	62.3	1550.0	75.2	73.7	59.3	86.8	42.3	15.9	75.9	47.5	59.0	66.3	65.8	58.5	60.1	65.1	67.1
Qwen2.5-7B+SigLIP2-So/16	DPO	68.9	1664.0	80.3	76.0	64.0	92.4	50.2	20.4	80.7	59.3	62.2	73.0	75.8	74.2	65.6	71.1	73.5
Qwen2.5-7B+SigLIP2-So/16	SFT	66.2	1627.7	78.6	74.9	59.9	91.8	48.7	18.7	79.9	46.0	63.5	71.9	72.3	68.8	64.0	69.0	70.0

Table R Scaling the language model in MLLMs. Using SigLIP2-So/16 as the vision encoder, we vary the size of the language model (Qwen2.5) and evaluate performance across multiple benchmarks.

			General				Knowledge				Vision-Centric				OCR & Chart			
Data size	Train	Average	MME^{P}	MMB	$SEED^{I}$	GQA	SQA^{I}	$MMMU^{V}$	$MathVista^{M}$	AI2D	MMVP	RealWorldQA	CV-Bench^{2D}	CV-Bench^{3D}	ChartQA	OCRBench	TextVQA	DocVQA
3K	DPO	60.4	1490.4	72.0	72.5	60.7	86.2	40.4	15.3	71.3	46.7	56.2	62.6	57.2	65.2	61.7	64.6	58.8
3K	SFT	56.4	1431.0	70.0	70.9	58.0	86.8	33.8	8.5	67.2	40.7	58.8	52.7	41.7	63.2	59.5	63.1	56.5
5K	DPO	60.6	1486.3	72.2	72.4	60.7	86.0	40.6	15.5	71.0	47.3	57.1	63.2	59.0	65.6	61.9	64.4	59.0
5K	SFT	57.6	1409.4	70.5	71.3	58.2	86.6	39.6	8.7	70.7	38.7	59.1	62.6	42.7	63.2	59.3	63.1	56.6
10K	DPO	60.8	1480.1	72.0	72.7	60.3	86.1	40.6	14.8	71.0	49.0	57.0	63.2	60.2	65.6	62.2	64.5	59.5
10K	SFT	58.9	1431.5	70.9	72.1	58.9	86.0	40.2	12.5	71.1	44.6	57.9	63.6	49.3	62.4	58.1	64.5	58.0
20K	DPO	61.0	1478.7	71.9	72.5	60.9	86.7	40.1	14.7	71.5	50.0	57.4	63.6	59.9	65.4	62.7	64.7	59.5
20K	SFT	59.1	1442.1	70.6	71.9	58.7	86.6	41.0	12.6	70.9	44.0	56.0	63.1	56.1	62.1	58.8	63.4	57.7
40K	DPO	61.3	1495.4	72.2	73.2	60.9	86.4	39.0	15.6	71.7	51.9	59.0	63.0	61.3	64.5	62.6	64.8	59.7
40K	SFT	59.5	1423.7	70.5	72.1	58.3	85.9	40.0	13.5	71.3	45.3	57.9	64.1	59.1	63.2	57.4	64.3	58.3

Table S Scaling data on MLLM performance. We vary the size of training data for an MLLM built with Qwen2.5-1.5B and SigLIP2-So/16 and measure its performance.

we use a 20K subset randomly sampled from the MMPR-1.2 dataset[8].

The hyperparameters for *Stage 1* are adopted from the standard LLaVA-OneVision finetuning script[9], including a learning rate of 1×10^{-5} and a batch size of 256. For *Stage 2* DPO post-training, we largely follow the corresponding script[10] but adjust the learning rate (LR) to 1×10^{-6} and use a batch size of 256 for our data scale. To ensure a controlled comparison for *Stage 2* SFT post-training, we use the same finetuning script with a learning rate of 5×10^{-6}, but remove the vision-encoder-specific LR, mirroring the DPO setup.

Since SFT and DPO rely on fundamentally different loss formulations, their optimal learning rates naturally diverge. In practice, we observe that DPO requires substantially smaller LRs than SFT, partly because DPO accounts for both chosen and rejected responses, effectively doubling the batch size per iteration compared to SFT. This observation aligns with prior settings, such as those in InternVL2.5 (Wang et al., 2024b), where an LR of 2×10^{-7} is used for DPO and 4×10^{-5} for SFT.

Benchmark	Task	Domain	Citation
GQA	all	General VQA	Hudson & Manning (2019)
SEED	image-based	General VQA	Ge et al. (2023)
MME	perception	General VQA	Fu et al. (2023)
MMBench	all	General VQA	Liu et al. (2024b)
AI2D	all	Knowledge VQA	Hiippala et al. (2021)
ScienceQA	image-based	Knowledge VQA	Lu et al. (2022)
MathVista	math	Knowledge VQA	Lu et al. (2023)
MMMU	vision	Knowledge VQA	Yue et al. (2024)
TextVQA	all	OCR & Chart VQA	Singh et al. (2019)
DocVQA	all	OCR & Chart VQA	Mathew et al. (2021)
ChartQA	all	OCR & Chart VQA	Masry et al. (2022)
OCRBench	all	OCR & Chart VQA	Liu et al. (2023b)
MMVP	all	Vision-Centric VQA	Tong et al. (2024b)
RealWorldQA	all	Vision-Centric VQA	xAI (2024)
CVBench-2D	all	Vision-Centric VQA	Tong et al. (2024a)
CVBench-3D	all	Vision-Centric VQA	Tong et al. (2024a)

Table T List of benchmarks used. To evaluate MLLMs, we use 16 benchmarks that are assigned to each of the domains proposed in Cambrian (Tong et al., 2024a).

E.2 Evaluation benchmarks

As stated in Section 3.1, we adopt the evaluation suite from Cambrian (Tong et al., 2024a) for a comprehensive assessment of MLLM performance. This suite consists of 16 benchmarks categorized into four domains: General, Knowledge, OCR & Chart, and Vision-Centric VQA. A list of these benchmarks, along with their domain assignments and citations, is provided in Table T. Unlike other benchmarks whose scores generally range from 0 to 100, MME produces values on a 0–2000 scale. To ensure comparability within the overall MLLM evaluation, when computing the average score, we rescale the MME results by a factor of 20. We utilize the Cambrian source code, except in the case of DocVQA (Mathew et al., 2021). The Cambrian implementation of DocVQA does not yield numeric outputs automatically; rather, it requires manual submission of result CSV files to the evaluation website. To streamline this process, we employ the lmms-eval (Zhang et al., 2024) source code to obtain DocVQA scores.

E.3 ImageNet classification

This section details the protocol for the ImageNet classification experiment presented in Section 4. Our approach is based on the linear probe evaluation from the official OpenAI-CLIP repository[11]. As recommended in their public issue[12], we freeze the feature extractor and train a scikit-learn Logistic Regression model with L2 regularization, sweeping over lambda values for a maximum of 1000 iterations. Since evaluating on the full 1M ImageNet dataset is time-consuming, we follow the practice discussed in the community[13] and perform validation on a 50k random subset of the ImageNet data for early-stage validation. In addition, we implement a prototype-based linear classifier for more rapid validation; this is achieved by averaging the features of each class to form the weights of a linear layer. We verify that this faster method yields similar performance trends to the standard Logistic Regression approach.

E.4 Grad-CAM

We present here the experimental details for the gradient visualization in Section 4. We construct a training pipeline using *a single sample* and visualize the gradients around the 20th step. This setup alleviates the issue where the cosine learning rate scheduler sets the initial learning rate near zero and

[8] https://huggingface.co/datasets/OpenGVLab/MMPR-v1.2
[9] https://github.com/LLaVA-VL/LLaVA-NeXT/blob/main/scripts/train/finetune_si.sh
[10] https://github.com/LLaVA-VL/LLaVA-NeXT/blob/main/scripts/train/dpo.sh
[11] https://github.com/openai/CLIP?tab=readme-ov-file#linear-probe-evaluation
[12] https://github.com/openai/CLIP/issues/39#issuecomment-778034767
[13] https://github.com/openai/CLIP/issues/64#issuecomment-804444364

produces uninformative gradients at very early steps in the original LLaVA-OneVision code. By focusing on this step range, we obtain meaningful gradient patterns.

E.5 Semantic segmentation

We describe here the experimental details for the semantic segmentation study in Section 4. The setup follows the implementation referenced in the codebase of prior work (Covert et al., 2025)[14]. Specifically, we freeze the vision encoder and attach a two-layer MLP head, which is trained on the ADE20K dataset (Zhou et al., 2017). Evaluation is conducted on the validation set, where segmentation is performed at the patch level and recall is used as the primary metric. The training procedure follows the default configuration of the referenced repository, including 5 training epochs and a learning rate of 1×10^{-3}.

E.6 Representation alignment

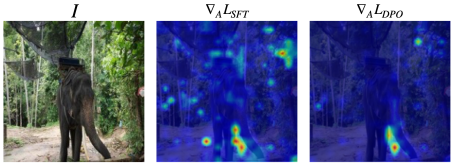
In Section 4, we present results measured against five reference LLMs, including Gemma-2B/7B (Team et al., 2024b), LLaMA-3-8B (Dubey et al., 2024), Mixtral-8x7B (Jung et al., 2010) and Bloomz-7B (Muennighoff et al., 1786). The vision models under analysis are vision encoders trained within MLLM frameworks alongside three different sizes of LLMs. We evaluate alignment between our vision encoders and the reference LLMs using the implementation provided in the Platonic Representation repository[15]. Scores are computed on the 'minhuh/prh' dataset distributed with the repository. Since this dataset contains only 1,024 examples, the results exhibit variability. To address this, we evaluate vision encoders trained with three different random seeds and report the averaged performance

E.7 PIVOT-enhanced vision model evaluation

To evaluate the effectiveness of PIVOT-enhanced vision models within MLLMs, we follow a pipeline consistent with prior evaluation protocols such as Cambrian (Tong et al., 2024a), DINO-MLLM (Fan et al., 2025), and MLLM-data (Han et al., 2025). The vision encoder first undergoes contrastive pretraining using CLIP or SigLIP on large-scale image–text data, then is optimized through preference-instructed finetuning (SFT and DPO) with 3M+20K samples, as described in Section 3.1 and Section E.1. For downstream MLLM training in Figure 11, the tuned vision encoder is frozen and coupled with a new LLM, Qwen-1.5B, then finetuned on the Cambrian 737K dataset using the configuration provided in the LLaVA-NeXT repository[16]. This setup includes a batch size of 256, a learning rate of 1×10^{-5}, and other default hyperparameters, allowing direct assessment of the standalone usefulness of vision representations within MLLMs.

[14] https://github.com/iancovert/patch-seg/tree/main?tab=readme-ov-file
[15] https://github.com/minyoungg/platonic-rep
[16] https://github.com/LLaVA-VL/LLaVA-NeXT/blob/main/scripts/train/finetune_si.sh

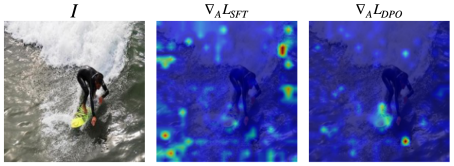
q · Does the elephant have tusks?



y_c · Yes, the elephant has tusks. They are visible in the image and appear to be a significant part of its physical appearance.

y_r · Yes, the elephant has tusks. They appear to be quite long and prominent, indicating that they have not been removed or damaged in any way.

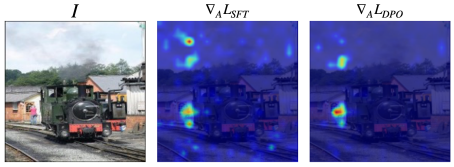
q · What colors make up the board? $A := \Phi_{ViT}(I)$



y_c · The board is black and yellow in color. This bright hue provides high visibility and stands out against the greenish-blue waters.

y_r · The board is made up of green colors. The use of these two colors may serve a practical or aesthetic purpose.

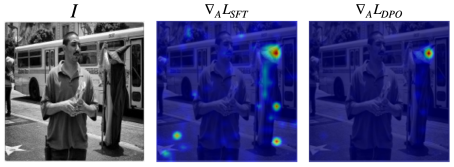
q · What color do you think the shirt is?



y_c · In the image, there is a person near the train who appears to be wearing a shirt. The color of the shirt worn by the individual seems to be red.

y_r · In the image, there is a person near the train who appears to be wearing a shirt. Upon closer inspection, the shirt seems to be blue.

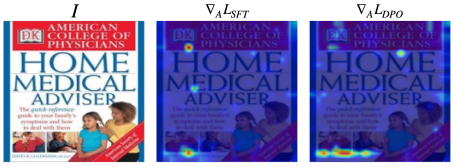
q · What type of headwear is the man in the background wearing?



y_c · The man in the background is wearing a wizard hat. This type of headwear is often associated with fantasy or role-playing themes, such as those found in popular culture, especially in the Harry Potter series.

y_r · The man in the background is wearing a wizard hat. This type of headwear features a conical shape and is typically made of fabric or felt material.

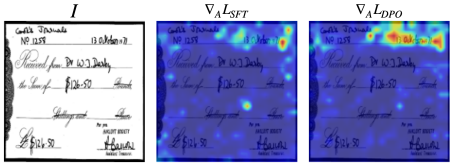
q · Who is the author of this book?



y_c · David R. Goldmann is the author of this book.

y_r · American Society of Interal Medicine is the author of this book.

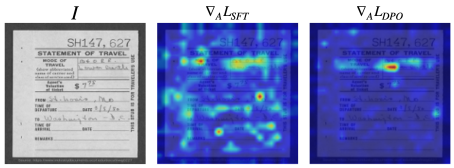
q · What is the date mentioned in the document?



y_c · The date mentioned in the document is 13 October 1971.

y_r · The date mentioned in the document is 13 November 1988.

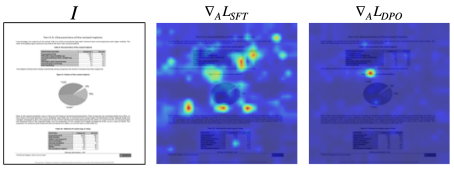
q · What is the stub for?



y_c · The stub is a "Statement of Travel" used to record details of a train journey, showing that the traveler used a Lower Berth in the sleeper car.

y_r · The stub serves as a record of the train trip, detailing the mode of transportation, fare, route, and relevant travel dates.

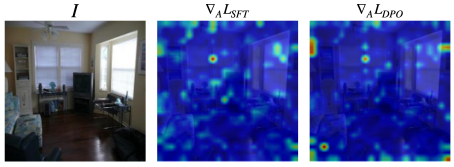
q · What is figure 8 title?



y_c · The title of Figure 8 is "Fixation of the revised implants". This figure is a pie chart illustrating the distribution of different types of fixation methods used in revised implants.

y_r · The title of Figure 8 is "Characteristics of the revised implants".

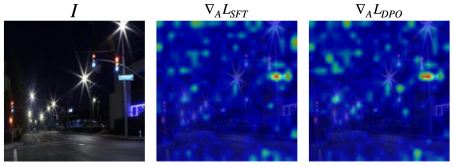
q · Please describe this photo in detail.



y_c · The image showcases a cozy living room setting. There's a television set on the left side, accompanied by various decorative items and books on its stand. On the right side of the TV, there are multiple wine glasses displayed.

y_r · The image showcases a living room setting. Several books can be found scattered around the room, some near the television and others towards the left side of the frame. The room has blinds covering the windows.

q · What are the main objects or subjects in the image? Please describe them in detail.



y_c · The image depicts a nighttime urban setting. There are multiple traffic lights scattered throughout the scene, illuminating the area with their colors. The sky is dark, suggesting it's late evening or during the night hours.

y_r · The image showcases a nighttime cityscape with multiple traffic lights, buildings, and street signs. There's a prominent intersection with several traffic lights. A fire hydrant is also visible on the right side of the road.

Figure E Additional results of Grad-CAM. We provide additional experimental results of Figure 7, where we illustrate the gradients received by the vision encoder under MLLM post-training approaches, DPO and SFT, using Grad-CAM (Selvaraju et al., 2017).



Figure F Qualitative results on segmentation probing. We study segmentation probing of a vision encoder (VE), CLIP-L/14 336px, post-trained in an MLLM with SFT and DPO, where Qwen2.5-3B is a base LLM. The DPO-trained ViT yields segmentation maps consistent with the ground truth, unlike the broader maps from the SFT-trained model.